PHILOSOPHICAL TRANSACTIONS OF THE ROYAL SOCIETY A MATHEMATICAL, PHYSICAL & ENGINEERING SCIENCES

On the Theory of Unsteady Shearing Flow over a Slot

M. S. Howe

Phil. Trans. R. Soc. Lond. A 1981 **303**, 151-180
doi: 10.1098/rsta.1981.0195

Phil. Trans. R. Soc. Lond. A **303**, 151–180 (1981) [151]
Printed in Great Britain

ON THE THEORY OF UNSTEADY SHEARING FLOW OVER A SLOT

By M. S. Howe
Bolt Beranek and Newman Inc., 50 Moulton Street, Cambridge, Massachusetts 02138, *U.S.A.*

(*Communicated by E. G. Broadbent, F.R.S. – Received 2 February* 1981)

CONTENTS

A linearized theory is proposed of the unstable motion of a thin shear layer formed in a slot in a thin, rigid plate by unequal, parallel mean flows on opposite sides of the plate. Liepmann's asymptotic displacement thickness representation of the influence of an unsteady boundary layer is used to model the quasi-periodic ejection of vorticity from the slot at its trailing edge. Discrete intervals in frequency are found within which energy is extracted from the mean flow by the unsteady motion in the slot. When the mean velocities on opposite sides of the plate approach a common, non-zero value, the number of these intervals increases without limit, indicating that perturbation energy is supplied by the mean flow even when the Kelvin–Helmholtz instabilities of a mean shear layer are absent. A detailed analysis of the motion in the general case reveals that the net flux of fluid through the slot is composed of a component q caused by the to-and-fro motion of the shear layer, together with a component q_h that accompanies the ejection of vorticity at the trailing edge. Except at very small Strouhal numbers, q and q_h are of almost equal magnitude but of opposite sign, so that the net flux arises from a delicate imbalance between these opposing flows, and amounts to a small fraction of either one.

Application of the theory is made to determine the influence of the ejected vorticity on the excitation of self-sustaining wall cavity oscillations, and on the diffraction of sound by a perforated screen. Such screens are used to attenuate aerodynamic sound

in cross-flow heat exchangers. The theory is compared with Ronneberger's (1980) detailed observations of the motion of a shear layer over a wall cavity. Acceptable agreement is obtained provided that, at the higher Strouhal numbers, the influence of the finite width of the shear layer is included in the calculation of the growth rates of the instability waves.

1. Introduction

A free shear layer in a nominally steady mean flow can execute large-amplitude fluctuation when small, mean flow inhomogeneities trigger the growth of Kelvin–Helmholtz instabilit waves. The subsequent motion is often quasi-periodic in time. The periodicity is associate with the existence of a source of feedback that initiates a new instability wave on the shea layer. Typical feedback sources are produced by: the pairing of discrete vortices formed in th layer; the impingement of the shear layer on an edge or other obstacle; the proximity of a acoustic resonator, such as a wall cavity; etc. An extensive survey and bibliography of thes and related phenomena is provided by the recent article by Rockwell & Naudascher (1979).

In a previous paper (Howe 1981*a*, hereafter referred to as I), a linearized theory was pro posed of unsteady shearing flow of a weakly compressible fluid over a two-dimensional slot i a thin rigid plate. Earlier treatments of this problem are discussed and referenced in I, t which the reader is referred for further details. The mean flow speed was equal to U 'above the plate (see figure 1), and vanished on the lower side; the shear layer within the slot wa modelled by a vortex sheet of infinitesimal thickness. The influence of viscosity was ignore except in so far as it must be invoked (as in thin aerofoil theory) to satisfy a Kutta conditio at the leading edge (A in figure 1) of the slot. The analytical representation obtained in I c the displacement ζ of the vortex sheet from its undisturbed position contains two disposabl constants, which determine the amplitudes of the Kelvin–Helmholtz instability waves. Whe these constants are chosen to ensure that the vortex sheet is attached ($\zeta = 0$) to the plate a the leading and trailing edges of the slot (A and B in figure 1), it was shown in I that ther can be no net exchange of energy between the mean flow and the unsteady motion throug the slot. Any small disturbance of the shear layer is accordingly damped in time. When, how ever, the constants are fixed by the Kutta condition that $\zeta, \partial\zeta/\partial x_1 = 0$ at A, where x_1 measured in the mean flow direction, it was predicted that energy can be extracted from th mean flow by disturbances satisfying $1.59 < \omega s/U < 3.49$, where ω is the radian frequenc of the motion and $2s$ is the width of the slot. These inequalities constitute a simple criterio for predicting, for example, the range of velocity U within which a wall-cavity resonance c frequency ω is excited, and experimental data cited in I give encouraging support for th particular model of the motion of the shear layer. Application of the Kutta condition leav conditions prevailing at the trailing edge B of the slot to be determined by the solution of th equations of motion, and it is found that the displacement ζ possesses a singularity proportion to the inverse square root of the distance from B. A relatively weak singularity of this type perfectly acceptable in a linear theory, since in practice the observed motion at the trailin edge is discontinuous and of large amplitude (a striking illustration of the behaviour is provide by figure 4 of Ronneberger (1980)).

A more serious objection to this earlier analysis is that it takes no account of vorticity periodi ally ejected from the slot on either side of the plate at the trailing edge. On the upper side c the slot such vorticity is convected in the mean flow and produces a large perturbation in th boundary layer downstream of the slot. Semi-empirical theories of the interaction of the shea

layer with the trailing edge, such as those proposed by Heller & Bliss (1975), Ronneberger (1972, 1980), and Tam & Block (1978), model the influence of the violent motion at the trailing edge by means of a dipole line source, located at B with the dipole axis perpendicular to the plate. This source is assumed to characterize the periodic ejection of vorticity.

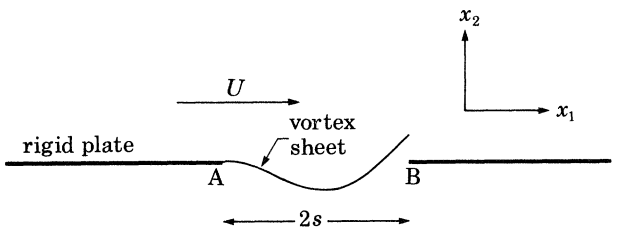

FIGURE 1. Schematic illustration of the problem considered in I.

In the present paper the theoretical discussion given in I is extended in two ways. First the basic mean flow is generalized to include the possibility of there being parallel mean flows on both sides of the plate (see figure 2). Second an asymptotic theory is introduced to account for the influence of the ejected vorticity. This is based on a proposal due to Liepmann (1954) for calculating the aerodynamic noise generated by a turbulent boundary layer (see also Laufer *et al.* 1964; Howe 1981*b*, *c*). Liepmann's idea is to represent the unsteady flow induced by the vorticity in the boundary layer in terms of the corresponding fluctuations in the boundary layer displacement thickness. A linearized theory cannot take explicit account of discrete vortices in the boundary layer, but it may be expected that their aggregate effect on the exterior fluid will be adequately represented by a superposition of harmonic *displacement thickness waves* that propagate downstream from the slot. This simplified version of the problem is still too difficult to treat analytically in full generality and, following Liepmann, we shall confine attention to the asymptotic case of small Strouhal number $\omega\delta/U \ll 1$, wherein the length scale of the displacement thickness waves is large relative to the width δ, say, of the boundary layer. In this limit the magnitude of the displacement thickness perturbation, which provides a boundary condition for the determination of the potential flow in the region outside the boundary layer, may be assumed to be specified *on the surfaces of the plate* downstream of the slot (cf. Howe 1981*b*).

The displacement thickness waves are generated at the trailing edge B of the slot, and their presence will be shown to furnish an additional disposable constant which can be chosen to remove the singularity in the displacement ζ of the shear layer that arises in the analysis given in I. An analogous condition has to be imposed in the theory of the flue organ pipe discussed by Howe (1981*b*), although the influence of the unstable free shear layers of the organ pipe jet are of less significance than in the slot problem. It was deduced in that study that displacement thickness waves excited by sound incident on the lip of the mouth of the organ pipe leads to a net gain of acoustic energy at the expense of that of the mean jet flow. This conclusion remains valid in the present case of unsteady shearing flow over a slot – vorticity ejected from the slot tends to promote the extraction of mean flow energy to support the fluctuations within the slot.

The asymptotic problem is formulated and solved in §2; the derivations of several analytical results are collected together in the Appendix. In §3 a general formula is derived for the rate at which acoustic energy is extracted from the mean flow. It is shown that as the mean shear across the slot is reduced, by causing the mean flow velocities on opposite sides of the plate to

approach a common, non-zero value, the Strouhal number interval $1.59 < \omega s/U < 3.49$ obtained in I within which energy is extracted from the mean flow is progressively augmented by a sequence of intervals at higher frequencies, which ultimately, when the flow velocities are the same, are of equal width and are spaced at equal intervals in frequency. Application of these results is made to determine the influence of vorticity ejection on the prediction given in I of the dependence on mean flow velocity of the frequency of self-sustained oscillations of a wall-cavity. An explicit representation is given in §4 for the displacement ζ of the vortex sheet, and the dependence of the profile on the magnitude of the mean shear is examined. In particular one finds that, as the length scale of the displacement thickness waves diminishes to zero, the limiting form assumed by ζ coincides with that predicted in I. This indicates that the back-reaction on the slot of displacement thickness waves that violate the asymptotic condition $\omega\delta/U \ll 1$ of the theory may not be significant in practice. The unsteady flux of fluid through the slot is partitioned between that due to the motion of the shear layer and a component associated with the ejection of vorticity at the trailing edge. It is shown (§4) that, except at very small Strouhal numbers, the component fluxes are of almost equal magnitude but are 180° out of phase; accordingly the net flux tends to be small compared with either of these components.

In §5 we consider the special case in which the mean flow velocities are the same on both sides of the plate. Comparison is made with an analysis of this problem given previously by the author (Howe 1980) which took no account of vorticity ejection, and predicted that the displacement ζ of the vortex sheet has a simple (finite) discontinuity at the trailing edge of the slot. It is argued that the present theory gives a more realistic modelling of the flow, and application is made to obtain the corresponding corrections to the results of Howe (1980) concerning the diffraction of sound by a perforated screen in a uniform mean grazing flow. The earlier practical predictions of the attenuation of sound by such a screen when placed, for example, in the cavity of a cross-flow heat exchanger, are shown to be only marginally modified. Finally, in §6 the theory is checked against the very recent experimental studies of Ronneberger (1980). When due account is taken of differences in the experimental and theoretical configurations, it can be concluded that acceptable agreement is obtained between the theoretical and measured profiles of the displacement ζ of the shear layer provided that, at the higher Strouhal numbers $\omega s/U$, the influence of the finite width of the shear layer is included in the computation of the growth rates of the Kelvin–Helmholtz instability waves.

2. Linear theory of unsteady shear flow over a slot

A thin rigid plate lies in the plane $x_2 = 0$ of a rectangular coordinate system (x_1, x_2, x_3) as in figure 2, with the x_3-axis directed out of the plane of the paper. A slot of width $2s$ occupies the portion $|x_1| < s$, $-\infty < x_3 < \infty$ of the plate, and in the undisturbed state the fluid is in motion parallel to the x_1-axis at speeds U_+, U_-, $U_+ \geqslant U_- > 0$, in $x_2 \gtrless \pm\delta$ respectively, where $\delta > 0$ is a characteristic boundary layer width. The shear layer in the slot has thickness of order 2δ which is taken to be small compared with $2s$. A uniform time-harmonic pressure $p_0 e^{-i\omega t}$ $(\omega > 0)$ is applied in the region $x_2 > 0$, and it is required to determine the subsequent motion of the system in the linearized approximation.

The sound speed c and the mean density ρ_0 are assumed to be constant throughout the flow, and we shall also require that

$$M^2 \ll 1, \quad ks \ll 1, \tag{2.1}$$

where $M = U_+/c$ is the Mach number of the flow in $x_2 > \delta$, and $k = \omega/c$ is the acoustic wavenumber. The characteristic acoustic wavelength is therefore large compared with the width of the slot. In the following the harmonic time factor $e^{-i\omega t}$ will not be explicitly displayed.

Consider a plane control surface Σ_+ (dashed line in figure 2*a*) parallel to the plate and at a distance δ from it, just outside the boundary layer on the upper surface. Let $Z_+(x_1)$ denote the x_2-component of the displacement of fluid particles lying in Σ_+ from their undisturbed positions.

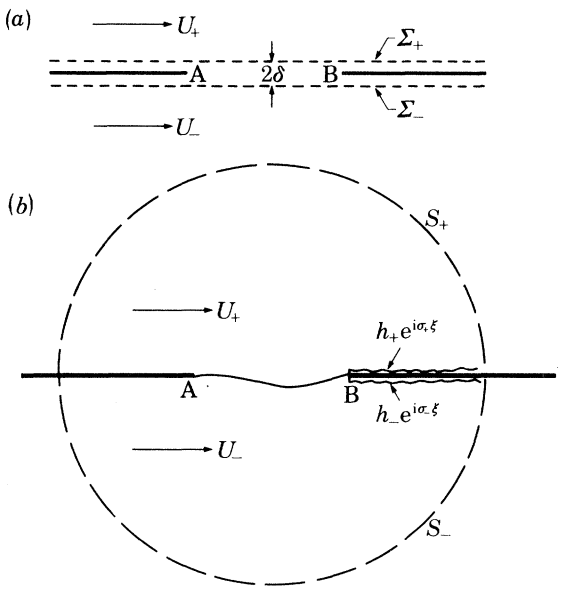

FIGURE 2. (*a*) Definition of the shear flow problem.
(*b*) The asymptotic idealization for $\omega\delta/U_+ \ll 1$.

As in I a Green function $G_+(\boldsymbol{x}, y_1)$ is introduced that satisfies the convected wave equation

$$\{(-ik + M_+\partial/\partial x_1)^2 - (\partial^2/\partial x_1^2 + \partial^2/\partial x_2^2)\}G_+(\boldsymbol{x}, y_1) = 0 \tag{2.2}$$

in $x_2 > \delta$, and the condition

$$\partial G_+/\partial x_2 = \delta(x_1 - y_1) \tag{2.3}$$

on $x_2 = \delta + 0$, $\delta(x)$ being the Dirac delta function. In specific applications G_+ must satisfy additional conditions, such as an appropriate radiation condition, and also take account of the possible existence of scattering centres on the plate at points remote from the slot.

The perturbation of the flow in $x_2 > \delta$ may be described by a potential ϕ_+, say, which can be expressed in terms of Z_+, G_+ by means of

$$\phi_+(\boldsymbol{x}) = \left(-i\omega + U_+\frac{\partial}{\partial x_1}\right)\int_{-\infty}^{\infty} Z_+(y_1)\,G_+(\boldsymbol{x}, y_1)\,dy_1, \tag{2.4}$$

(cf. equation (2.6) of I). By making use of the linearized form of Bernoulli's equation $p_+/\rho_0 + (-i\omega + U_+\partial/\partial x_1)\phi_+ = 0$, it follows that the total perturbation pressure p_+ in $x_2 > \delta$ can be expressed as

$$p_+ = -\rho_0\left(-i\omega + U_+\frac{\partial}{\partial x_1}\right)^2\int_{-\infty}^{\infty} Z_+(y_1)\,G_+(\boldsymbol{x}, y_1)\,dy_1 + p_0. \tag{2.5}$$

Similarly, in $x_2 < -\delta$ we have:

$$p_- = -\rho_0\left(-\mathrm{i}\omega + U_-\frac{\partial}{\partial x_1}\right)^2 \int_{-\infty}^{\infty} Z_-(y_1)\, G_-(x, y_1)\, \mathrm{d}y_1, \tag{2.6}$$

where $Z_-(x_1)$ is the x_2-component of the displacement of fluid particles lying in the plane Σ_- of figure 2*a*, and, in $x_2 < -\delta$, $G_-(x, y_1)$ satisfies (2.2) with U_+ replaced by U_- and is such that $\partial G_-/\partial x_2 = -\delta(x_1 - y_1)$ on $x_2 = -\delta - 0$.

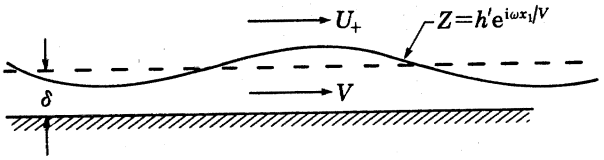

FIGURE 3. A neutrally stable displacement thickness wave of constant form satisfying $\omega\delta/U_+ \ll 1$ propagates at speed V on a vortex sheet that separates the mean stream from a uniform wall flow at speed V.

We now introduce the hypothesis that the displacements $Z_\pm$ and the boundary layer width δ are small compared with the length scale of variation, U_+/ω, of the motion. It may then be assumed that, for $|x_1| < s$,

$$\left.\begin{aligned} Z_+(x_1) &= Z_-(x_1) = Z(x_1), \\ p_+ &= p_-, \end{aligned}\right\} \tag{2.7}$$

since the relative magnitudes of inertia forces associated with the motion of the shear layer in the slot are proportional to $\omega^2\delta Z/U_+^2 \ll 1$. This is equivalent to replacing the shear layer within the slot by a vortex sheet. In this same asymptotic limit, the control surfaces $\Sigma_\pm$ may be taken to coincide respectively with $x_2 = \pm 0$. The second of equations (2.7) therefore implies that, for $|x_1| < s$:

$$\left(\omega + \mathrm{i}U_-\frac{\partial}{\partial x_1}\right)^2 \int_{-\infty}^{\infty} Z_-(y_1)\, G_-(x_1, -0, y_1)\, \mathrm{d}y_1 - \left(\omega + \mathrm{i}U_+\frac{\partial}{\partial x_1}\right)^2 \int_{-\infty}^{\infty} Z_+(y_1)\, G_+(x_1, +0, y_1)\, \mathrm{d}y_1 = -\frac{p_0}{\rho_0}. \tag{2.8}$$

On the surfaces $\Sigma_\pm$ downstream of the slot ($x_1 > s$), $Z_\pm$ represent the displacement of fluid particles just outside the boundary layers. It will here be assumed that an adequate approximation to these displacement thickness fluctuations is provided by the sinusoidal waveforms

$$Z_+ = h'_+\mathrm{e}^{\mathrm{i}\kappa_+ x_1}, \quad Z_- = h'_-\mathrm{e}^{\mathrm{i}\kappa_- x_1}, \tag{2.9}$$

where $h'_\pm$ are constant, and the wavenumbers $\kappa_\pm$ are determined by the mean velocity profiles of the boundary layers. In general, for a given frequency $\omega > 0$, a wall shear layer can support many such waves corresponding to a spectrum of values of $\kappa_\pm$. However, the analysis of simple model problems indicates that as $\omega\delta/U_\pm \to 0$ all possible wave modes coalesce (see, for example, Betchov & Criminale 1967), and this will be taken to justify the use of (2.9). Figure 3 illustrates such a representation of displacement thickness waves on an idealized 'top hat' mean velocity profile. The mean velocity is equal to U_+ for $x_2 > \delta$ and V for $0 < x_2 < \delta$. As $\omega\delta/U_+ \to 0$ it may be shown that $\kappa_+ \to \omega/V$.

The boundary layer displacement thickness waves propagate in the direction of the mean flow. In general it may therefore be assumed that $Z_\pm$ vanish in the region upstream of the slot

($x_1 < -s$). It would be necessary to relax this condition if boundary layer disturbances were known to be generated elsewhere in the flow and to be subsequently incident on the slot. In practice, the present hypothesis is equivalent to assuming that any such waves that *are* incident from upstream are *uncorrelated* with the applied pressure p_0, and may accordingly be treated separately in a linearized approximation.

To simplify the integro-differential equation (2.8) we introduce the dimensionless variables

$$\left.\begin{aligned} \xi &= x_1/s, & \eta &= y_1/s; \\ \zeta &= Z/s, & \zeta_\pm &= Z_\pm/s; \\ \epsilon_\pm &= \omega s/U_\pm, & \nu &= U_-/U_+. \end{aligned}\right\} \tag{2.10}$$

It will often be convenient to omit the suffix + from ϵ_+, and ϵ, ϵ_+ will be used interchangeably in the latter sections of this paper.

According to (2.9) we have in $\xi > 1$:

$$\left.\begin{aligned} \zeta_\pm &= h_\pm e^{i\sigma_\pm \xi}, \\ h_\pm &= h'_\pm/s, \quad \sigma_\pm = s\kappa_\pm \end{aligned}\right\}. \tag{2.11}$$

where

Conservation of matter does not permit the constants $h_\pm$ to be specified independently. Indeed, when quantities of $O(M^2)$ relative to unity are neglected, it follows from the equation of continuity that there can be no net flux of fluid away from the plate, so that

$$\int_{-\infty}^{\infty} \left(-i\omega + U_+ \frac{\partial}{\partial x_1}\right) Z_+(x_1)\, dx_1 = \int_{-\infty}^{\infty} \left(-i\omega + U_- \frac{\partial}{\partial x_1}\right) Z_1(x_1)\, dx_1. \tag{2.12}$$

Recall that $Z_\pm = 0$ for $x_1 < -s$. The convergence of the integrals in (2.12) as $x_1 \to +\infty$ is ensured by the causality condition. This requires that $Z_\pm$ should be regular functions of ω in the upper half-plane, and may be assumed to vanish as $\mathrm{Im}\,\omega \to +\infty$. Hence, when $\mathrm{Im}\,\omega$ is sufficiently large and positive, $\mathrm{Im}\,\sigma_\pm$ must also be large and positive. The integrals can therefore be evaluated for such ω, and their values as $\mathrm{Im}\,(\omega) \to +0$ obtained by analytic continuation. In this way one deduces that

$$h_+ e^{i\sigma_+}/\sigma_+ = h_- e^{i\sigma_-}/\sigma_- = -iq_h, \quad \text{say.} \tag{2.13}$$

Note that the above argument remains valid if $\mathrm{Im}\,(\sigma_\pm) < 0$ when ω is real, i.e. in the event that the displacement thickness waves are unstable and grow exponentially with distance downstream of the slot. The back-reaction of such waves on the motion in the slot is therefore seen to be finite. This treatment of instabilities may be contrasted with that recently advanced by Dowling *et al.* (1978), who deliberately suppress instability modes on the grounds that the linearized solution should be bounded everywhere. However, the author has shown in a recent study (Howe 1981*d*) that the application of such a procedure would result in there being no effective back-reaction of the displacement thickness waves on the motion in the slot.

The dimensionless flux Q of fluid through the slot into $x_2 > \delta$ is defined by

$$\left.\begin{aligned} Q &= q + q_h; \\ q &= \int_{-1}^{1} \zeta(\xi)\, d\xi, \quad q_h = \int_{+1}^{\infty} \zeta_\pm(\xi)\, d\xi \end{aligned}\right\}. \tag{2.14}$$

The component q represents the fluid displaced by the motion of the vortex sheet. The second term q_h is the flux due to the displacement thickness fluctuations downstream of the slot, and

is associated with the flow through the slot that occurs during the formation of the displacement thickness waves. This flow takes place in a region whose dimension is comparable with the characteristic scale δ of the mean shear layers. The present asymptotic analysis cannot resolve the details of structures of this size, so the flow appears to occur within an infinitesimal interval of the ξ-axis at the trailing edge.

When the inequalities (2.1) are fulfilled, $G_\pm(x, y_1)$ assume a common form in the acoustic near field of the slot:

$$\left.\begin{aligned} G_\pm(x, y_1) &= \pi^{-1}\ln\left[\{(x_1-y_1)^2+x_2^2\}^{\frac{1}{2}}/s\right]+a_\pm, \\ \text{so that, in particular,}\quad G_\pm(x_1, \pm 0, y_1) &\equiv G_\pm(\xi,\eta) = \pi^{-1}\ln|\xi-\eta|+a_\pm, \end{aligned}\right\} \tag{2.15}$$

where $a_\pm$ are complex constants (particular examples are discussed in I). Substituting into equation (2.8), and making use of the definitions (2.10), (2.11), (2.14), we find that the displacement of the vortex sheet satisfies

$$\begin{aligned} &\left\{\left(\epsilon_+ + \mathrm{i}\frac{\partial}{\partial\xi}\right)^2 + \nu^2\left(\epsilon_- + \mathrm{i}\frac{\partial}{\partial\xi}\right)^2\right\}\int_{-1}^{1}\zeta(\eta)\ln|\xi-\eta|\,\mathrm{d}\eta \\ &\quad = -\pi\{Q\epsilon_+^2(a_+ + a_-) + p_0/\rho_0 U_+^2\} - \left(\epsilon_+ + \mathrm{i}\frac{\partial}{\partial\xi}\right)^2\int_1^\infty h_+ \mathrm{e}^{\mathrm{i}\sigma_+\eta}\ln|\xi-\eta|\,\mathrm{d}\eta \\ &\quad\quad - \nu^2\left(\epsilon_- + \mathrm{i}\frac{\partial}{\partial\xi}\right)^2\int_1^\infty h_- \mathrm{e}^{\mathrm{i}\sigma_-\eta}\ln|\xi-\eta|\,\mathrm{d}\eta \quad (|\xi| < 1). \end{aligned} \tag{2.16}$$

The right-hand side of this equation may be simplified by making use of the integral identity

$$\int_1^\infty (h_+\mathrm{e}^{\mathrm{i}\sigma_+\eta} - h_-\mathrm{e}^{\mathrm{i}\sigma_-\eta})\ln|\xi-\eta|\,\mathrm{d}\eta = \mathrm{i}h_+\mathrm{e}^{\mathrm{i}\sigma_+}(1-\sigma_-/\sigma_+)\int_0^\infty \frac{\mathrm{e}^{\mathrm{i}k(\xi-1)}\mathrm{d}k}{(k-\sigma_-)(k-\sigma_+)}, \tag{2.17}$$

in which use has been made of (2.13), and where it may be temporarily assumed, as above, that $\mathrm{Im}\,\sigma_\pm > 0$. We now have

$$\begin{aligned} &\left\{\left(\epsilon_+ + \mathrm{i}\frac{\partial}{\partial\xi}\right)^2 + \nu^2\left(\epsilon_- + \mathrm{i}\frac{\partial}{\partial\xi}\right)^2\right\}\int_{-1}^{1}\zeta(\eta)\ln|\xi-\eta|\,\mathrm{d}\eta \\ &\quad = -\pi\{Q\epsilon_+^2(a_+ + a_-) + p_0/\rho_0 U_+^2\} - \left\{\left(\epsilon_+ + \mathrm{i}\frac{\partial}{\partial\xi}\right)^2 + \nu^2\left(\epsilon_- + \mathrm{i}\frac{\partial}{\partial\xi}\right)^2\right\}\int_1^\infty h_+\mathrm{e}^{\mathrm{i}\sigma_+\eta}\ln|\xi-\eta\,\mathrm{d}\eta \\ &\quad\quad + \mathrm{i}h_+\nu^2\mathrm{e}^{\mathrm{i}\sigma_+}\left(1-\frac{\sigma_-}{\sigma_+}\right)\left(\epsilon_- + \mathrm{i}\frac{\partial}{\partial\xi}\right)^2\int_0^\infty \frac{\mathrm{e}^{\mathrm{i}k(\xi-1)}\mathrm{d}k}{(k-\sigma_-)(k-\sigma_+)} \quad (|\xi| < 1). \end{aligned} \tag{2.18}$$

Integration with respect to the differential operator in the curly brackets on the left side yields

$$\int_{-1}^{1}\zeta(\eta)\ln|\xi-\eta|\,\mathrm{d}\eta = \chi(\xi) \quad (|\xi| < 1), \tag{2.19}$$

in which

$$\begin{aligned} \chi(\xi) &= -\tfrac{1}{2}\pi\{Q(a_+ + a_-) + p_0/\rho_0\epsilon_+^2 U_+^2\} + \alpha\mathrm{e}^{\mathrm{i}\epsilon_1\xi} + \beta\mathrm{e}^{\mathrm{i}\epsilon_2\xi} - \int_1^\infty h_+\mathrm{e}^{\mathrm{i}\sigma_+\eta}\ln|\xi-\eta|\,\mathrm{d}\eta \\ &\quad + \mathrm{i}h_+\nu^2\mathrm{e}^{\mathrm{i}\sigma_+}\left(1-\frac{\sigma_-}{\sigma_+}\right)\int_0^\infty \frac{(k-\epsilon_-)^2\mathrm{e}^{\mathrm{i}k(\xi-1)}\mathrm{d}k}{f(k)}, \end{aligned} \tag{2.20}$$

$$f(k) = (k-\sigma_-)(k-\sigma_+)\{(k-\epsilon_+)^2 + \nu^2(k-\epsilon_-)^2\}, \tag{2.21}$$

and $\epsilon_{1,2}$ are given by:

$$\epsilon_1 = \epsilon(1+\mathrm{i})/(1+\mathrm{i}\nu), \quad \epsilon_2 = \epsilon(1-\mathrm{i})/(1-\mathrm{i}\nu). \tag{2.22}$$

As in the corresponding equation (2.18) of I, α and β denote the amplitudes of the Kelvin–Helmholtz waves of the vortex sheet in the slot characterized by the conjugate wavenumbers

$\epsilon_{1,2}$. The influence of the displacement thickness waves is contained in the terms in $\chi(\xi)$ that involve h_+.

The integral equation (2.19) determines the displacement ζ of the vortex sheet in terms of the applied pressure p_0 and the three parameters α, β, h_+; the flux Q can be calculated in terms of these quantities from its definition (2.14). The values of α, β, h_+ will be chosen to satisfy the Kutta condition at the leading edge of the slot, and such that ζ remains finite at the trailing edge, i.e. we shall require that

$$\left.\begin{aligned} \zeta(\xi), \quad \partial\zeta(\xi)/\partial\xi \to 0 \quad \text{as} \quad \xi \to -1+0, \\ \zeta(\xi) < \infty \quad \text{as} \quad \xi \to +1-0. \end{aligned}\right\} \tag{2.23}$$

The solution of (2.19) may be expressed in the form (Carrier *et al.* 1966, p. 428)

$$\zeta = \{\pi(1-\xi^2)^{\frac{1}{2}}\}^{-1}\{\Theta_1(\chi, \xi) - \Theta_0(\chi)/\ln 2\} \quad (|\xi| < 1), \tag{2.24}$$

where $\Theta_0(\chi)$, $\Theta_1(\chi, \xi)$ are linear functionals defined by

$$\left.\begin{aligned} \Theta_0(\chi) &= \frac{1}{\pi}\int_{-1}^{1} \frac{\chi(\eta)\,\mathrm{d}\eta}{(1-\eta^2)^{\frac{1}{2}}}, \\ \Theta_1(\chi, \xi) &= \frac{1}{\pi}\int\!\!\!\!\!\!-_{-1}^{1} \frac{(1-\eta^2)^{\frac{1}{2}}\chi'(\eta)\,\mathrm{d}\eta}{\eta-\xi}, \end{aligned}\right\} \tag{2.25}$$

the second integral being a principal value, and $\chi'(\eta) = \partial\chi/\partial\eta$.

Integrating equation (2.24) with respect to ξ over $(-1, 1)$, and noting that the contribution from the principal-value integral vanishes, we find

$$q \ln 2 + \Theta_0(\chi) = 0. \tag{2.26a}$$

This result may be used to express the conditions that ζ should remain finite or vanish as $\xi \to \mp 1 \pm 0$ in the form

$$\lim_{\xi \to \mp 1 \pm 0} \{q + \Theta_1(\chi, \xi)\} = 0. \tag{2.26b, c}$$

The Kutta condition will be satisfied provided that

$$\lim_{\xi \to -1+0} \{\partial\Theta_1(\chi, \xi)/\partial\xi\} = 0. \tag{2.26d}$$

These equations determine the constants q, α, β, h_+ in terms of the applied pressure p_0. The details are given in the Appendix, where the integrals appearing in (2.26*a–d*) are also evaluated. At this point it is sufficient to quote the result for the net flux Q, defined in (2.14), namely

$$Q\{\ln 2 - \tfrac{1}{2}\pi(a_+ + a_-) + F(\epsilon)\} = \pi p_0/2\rho_0\epsilon_+^2 U_+^2. \tag{2.27}$$

The complex-valued function $F(\epsilon)$ is defined in terms of $\epsilon_{1,2}$, $\sigma_\pm$ and the Bessel and Hankel functions J_n, $H_n^{(1)}$ by means of

$$\begin{aligned} F(\epsilon) = [[&[J_0(\epsilon_1) - \epsilon_1(\mathscr{H}_0/\mathscr{F})\{J_0(\epsilon_1) - \mathrm{i}J_1(\epsilon_1)\}][(1/\epsilon_2 - 1/\sigma_+)J_0(\epsilon_2) \\ &+ \epsilon_2(G/\mathscr{F})\{J_0(\epsilon_2) - \mathrm{i}J_1(\epsilon_2)\}] - [J_0(\epsilon_2) - \epsilon_2(\mathscr{H}_0/\mathscr{F})\{J_0(\epsilon_2) - \mathrm{i}J_1(\epsilon_2)\}] \\ &\times [(1/\epsilon_1 - 1/\sigma_+)J_0(\epsilon_1) + \epsilon_1(G/\mathscr{F})\{J_0(\epsilon_1) - \mathrm{i}J_1(\epsilon_1)\}]]/\Delta, \end{aligned} \tag{2.28}$$

where

$$\begin{aligned} \Delta = {} & J_0(\epsilon_2)J_1(\epsilon_1) - J_0(\epsilon_1)J_1(\epsilon_2) \\ & + (\epsilon_1/\mathscr{F})\{\mathscr{H}_0 J_1(\epsilon_2) - \mathscr{H}_1 J_0(\epsilon_2)\}\{J_0(\epsilon_1) - \mathrm{i}J_1(\epsilon_1)\} \\ & - (\epsilon_2/\mathscr{F})\{\mathscr{H}_0 J_1(\epsilon_1) - \mathscr{H}_1 J_0(\epsilon_1)\}\{J_0(\epsilon_2) - \mathrm{i}J_1(\epsilon_2)\}; \end{aligned} \tag{2.29}$$

$$\mathscr{F} = \sigma_+\{H_0^{(1)}(\sigma_+) - \mathrm{i}H_1^{(1)}(\sigma_+)\} - \nu^2(1-\sigma_-/\sigma_+)\sum_{j=1}^{4}\frac{\sigma_j^2(\sigma_j-\epsilon_-)^2}{f_j'}\{H_0^{(1)}(\sigma_j) - \mathrm{i}H_1^{(1)}(\sigma_j)\}\,\mathrm{e}^{\mathrm{i}(\sigma_+-\sigma_j)}; \tag{2.30}$$

$$G = \nu^2(1-\sigma_-/\sigma_+)\sum_{j=1}^{4}(1-\sigma_j/\sigma_+)(\sigma_j-\epsilon_-)^2 H_0^{(1)}(\sigma_j)\,\mathrm{e}^{\mathrm{i}(\sigma_+-\sigma_j)}/f_j'; \tag{2.31}$$

$$\mathscr{H}_n = H_n^{(1)}(\sigma_+) - \nu^2(1-\sigma_-/\sigma_+)\sum_{j=1}^{4}\sigma_j(\sigma_j-\epsilon_-)^2 H_n^{(1)}(\sigma_j)\,\mathrm{e}^{\mathrm{i}(\sigma_+-\sigma_j)}/f_j' \quad (n = 0, 1). \tag{2.32}$$

In (2.30)–(2.32) the shorthand notation σ_j ($j = 1, 2, 3, 4$) has been introduced:

$$\left.\begin{aligned}&\sigma_1 = \sigma_+, \quad \sigma_2 = \sigma_-, \quad \sigma_3 = \epsilon_1, \quad \sigma_4 = \epsilon_2;\\ \text{and}\qquad &f_j' = (\partial f/\partial k)_{k=\sigma_j}.\end{aligned}\right\} \tag{2.33}$$

Equation (2.27) has the same structure as the corresponding equation (2.28) of I, and it is shown in the Appendix that the functional form of $F(\epsilon)$ reduces to that given in I (equation (2.29)) when $\nu = 0$ and $|\sigma_\pm| \to \infty$. As this limit is approached the wavelengths of the boundary layer displacement thickness waves diminish to zero and, except at the trailing edge $\xi = 1$ of the slot, there is effective cancellation of the velocities induced in the flow by the successive elements of the displacement thickness fluctuations.

3. Extraction of energy from the mean flow

The mechanical energy in the neighbourhood of the slot is partitioned between (i) the kinetic energy of the mean flow; (ii) the kinetic energy of the essentially incompressible perturbations associated with the near fields of the displacement thickness waves and the vortex sheet within the slot; and (iii) the energy stored in the mechanism responsible for the applied pressure p_0. The displacement thickness waves transport kinetic energy away from the slot, and in the absence of further interactions (in particular when the relatively weak quadrupole coupling with the acoustic field is neglected) that energy remains localized near the boundary layer. The applied pressure p_0 will usually represent a sound wave incident on the slot, and it is convenient, henceforth, to refer to it in these terms, although it could equally well characterize a large-scale, incompressible disturbance (an 'evanescent' sound wave). This incident acoustic energy may be partially absorbed by the vorticity field during the formation of the displacement thickness fluctuations. Alternatively, the interaction with the slot of unsteady vorticity within the slot may result in a net gain in acoustic energy. In such circumstances the mean flow must be the ultimate source of this additional energy. We now establish a general result (stated without proof in I) that acoustic energy is extracted from the mean flow at Strouhal numbers $\epsilon = \omega s/U_+$ satisfying $\mathrm{Im}\{F(\epsilon)\} < 0$.

Consider the flux of acoustic energy through the semicircular cylindrical control surfaces $S_\pm$ of figure 2*b* whose common radius $r \gg s$, and satisfies also $kr \ll 1$, so that the acoustic wavelength greatly exceeds r. Let v_n denote the component of the acoustic perturbation velocity in the direction of the outward normal to S_+, and let Π_+ be the net acoustic energy flux through S_+ away from the slot per unit length in the x_3-direction. Then

$$\Pi_+ = r\int_0^\pi \langle p_+ v_n\rangle \,\mathrm{d}\theta, \tag{3.1}$$

where (r, θ) are polar coordinates of a point on S_+, and the angle brackets denote an average over a wave period $2\pi/\omega$. Equation (3.1) neglects a possible contribution to the energy flux due to convection of sound by the mean flow. This would give an additional component that is $O(M^2)$ relative to (3.1) and is therefore neglected (see, for example, Ffowcs Williams & Lovely 1975).

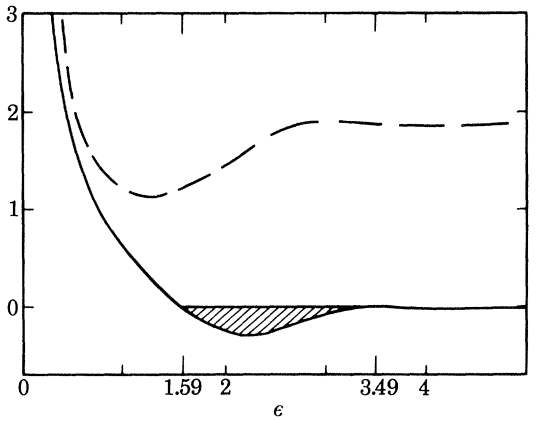

FIGURE 4. Variation of the real and imaginary parts of $F(\epsilon)$ for $\nu = 0$, $\sigma_\pm \to \infty$ (no displacement thickness waves): – – –, $-\mathrm{Re}\, F$; ——, $\mathrm{Im}\, F$.

Using the definition (2.5) of p_+ together with the explicit representation (2.15) of $G_+(\boldsymbol{x}, y_1)$, it follows that, for $r \equiv |\boldsymbol{x}| \gg s$,

$$p_+ \simeq \rho_0\omega^2 s^2\{\pi^{-1}\ln(r/s) + a_+\}\int_{-1}^{\infty}\zeta_+(\eta)\,\mathrm{d}\eta + p_0$$
$$\equiv \rho_0\omega^2 s^2 Q\{\pi^{-1}\ln(r/s) + a_+\} + p_0, \tag{3.2}$$

in which the definition (2.14) of Q has been used. Next, equations (2.4), (2.15) show that for $r \gg s$, the slot-induced flow is equivalent to that of a monopole source for which

$$v_n = \partial\phi_+/\partial r \simeq -\mathrm{i}\omega s^2 Q/\pi r. \tag{3.3}$$

To evaluate the integral in (3.1) we must first restore the harmonic time factor $\mathrm{e}^{-\mathrm{i}\omega t}$ in the definitions of p_+, v_n and take the real parts of the resulting expressions. In this way we find

$$\Pi_+ = \tfrac{1}{4}\rho_0\omega s^2\{\mathrm{i}((\omega s)^2|Q|^2 a_+ + p_0 Q^*/\rho_0) + \text{c.c.}\}, \tag{3.4}$$

where c.c. denotes the complex conjugate of the preceeding quantity, and an asterisk denotes the complex conjugate of a variable.

Similarly, the corresponding flux of acoustic energy away from the slot through S_- is found to be

$$\Pi_- = \tfrac{1}{4}\mathrm{i}\rho_0\omega^3 s^4|Q|^2 a_- + \text{c.c.} \tag{3.5}$$

Adding (3.4), (3.5) and using (2.27) to express p_0/ρ_0 in terms of Q, we find that the net rate of production of acoustic energy, Π, say, at the slot, is given by

$$\Pi = \Pi_+ + \Pi_-$$
$$= -\pi^{-1}\rho_0 s(\omega s)^3|Q|^2\,\mathrm{Im}\,\{F(\epsilon)\} \quad (\omega > 0), \tag{3.6}$$

and therefore that a net gain of acoustic energy occurs at the slot provided that $\mathrm{Im}\,\{F(\epsilon)\} < 0$.

In the general case discussed in I, $\nu = 0$ and $|\sigma_\pm| \to \infty$ (absence of displacement thickness waves), and figure 4 illustrates the corresponding dependence of $F(\epsilon)$ on real values of $\epsilon = \omega s/U_+$.

In the cross-hatched region Im $\{F(\epsilon)\} < 0$ and $1.59 < \epsilon < 3.49$. To assess the influence c the displacement thickness fluctuations and the mean shear ν, it is necessary to specify th relation between the wavenumbers $\sigma_{\pm}$ and the Strouhal number ϵ. This is determined by th mean velocity profiles of the boundary layers. Large-scale boundary layer disturbance characteristically convect at about 60 % of the mean stream velocity (cf. Bull 1967, Blak

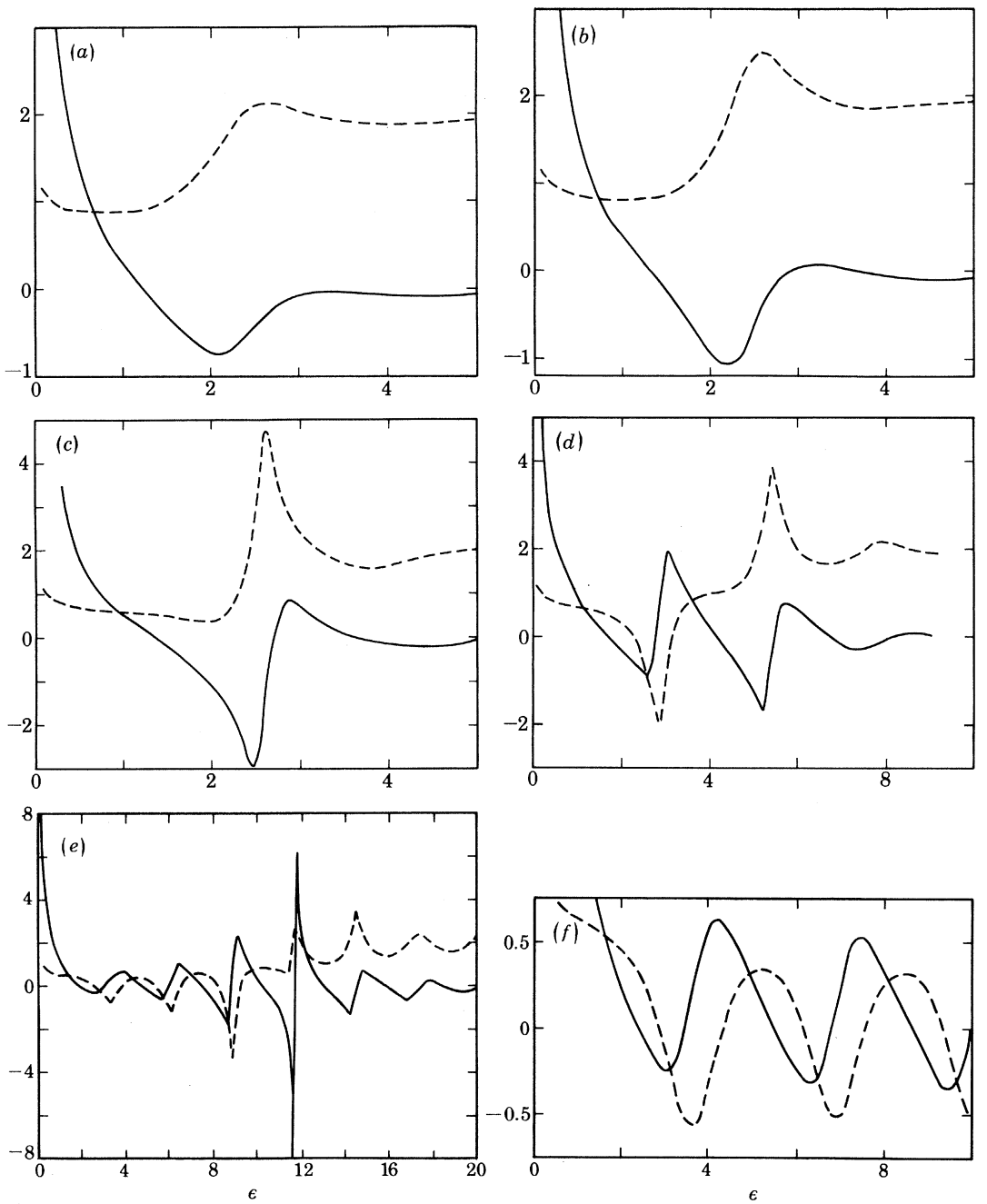

FIGURE 5. Variation of the real and imaginary parts of $F(\epsilon)$ with $\epsilon = \omega s/U_+$ (– – –, $-\mathrm{Re}\,F$; ——, Im F) wh the displacement thickness waves propagate according to (3.7) at 60 % of the local mean stream velocit (*a*) $\nu = 0$; (*b*) $\nu = 0.1$; (*c*) $\nu = 0.25$; (*d*) $\nu = 0.5$; (*e*) $\nu = 0.75$; (*f*) $\nu = 1$.

PHILOSOPHICAL TRANSACTIONS OF THE ROYAL SOCIETY A MATHEMATICAL, PHYSICAL & ENGINEERING SCIENCES

1970), and our theoretical results will therefore be illustrated for this case. We shall assume, in fact, that $\sigma_\pm = 5\omega s/3U_\pm$, i.e.

$$\sigma_+ = 5\epsilon/3, \quad \sigma_- = 5\epsilon/3\nu, \tag{3.7}$$

Figures 5*a–f* indicate the variations of $F(\epsilon)$ calculated from equation (2.28) for $\nu = 0$, 0.1, 0.25, 0.5, 0.75, 1 respectively, and for the $\sigma_\pm$ defined by (3.7). Observe that $\sigma_- \to \infty$ as $\nu \to 0$, and there is in this case no effective contribution from the displacement thickness waves on the lower side of the plate. A comparison of figures 4 and 5*a* shows how the conclusions of I are altered by the presence of the displacement thickness fluctuations. In particular, the

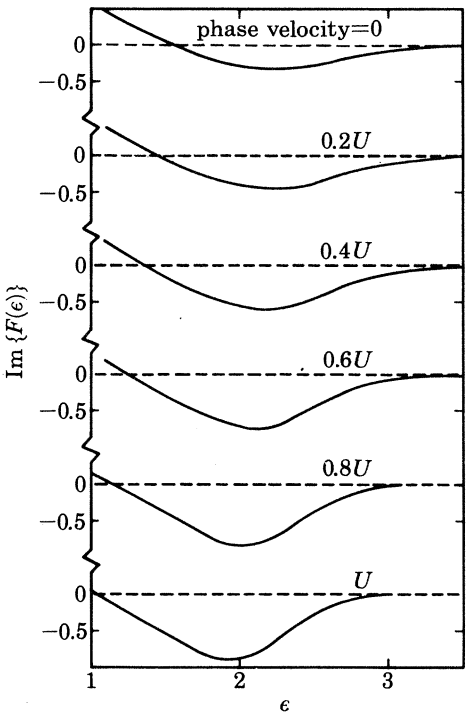

FIGURE 6. Variation of Im $\{F(\epsilon)\}$ for $1 \leqslant \epsilon \leqslant 3.5$, $\nu = 0$, and for different values of the phase velocity of boundary layer disturbances.

principal region in which Im $\{F(\epsilon)\} < 0$ now corresponds to the Strouhal number interval $1.23 < \epsilon < 3.27$, and the magnitude of the minimum value attained by Im F (≈ -0.72) is significantly greater than in figure 4. These differences have important consequences in the application of the theory to self-sustained oscillations of a wall-cavity, and are discussed in more detail below. For a given value of the net flux Q it appears from (3.6) that the influence of vorticity ejected from the slot, which is here modelled by the displacement thickness waves, is to *increase* the rate at which acoustic energy is extracted from the mean flow. This conclusion could, of course, depend on the choice (3.7) of the phase velocities of the boundary layer disturbances, but figure 6 reveals that, for $\nu = 0$, the peak value attained by $-$Im $\{F(\epsilon)\}$ in the range $1 < \epsilon < 3.5$ gradually increases as the phase velocity increases from zero to U_+ (corresponding to $\infty \geqslant \sigma_+ \geqslant \epsilon$).

It may be shown from the defining equations (2.28)–(2.32) of $F(\epsilon)$ that, for $\nu < 1$,

$$F(\epsilon) \to -2 \quad \text{as} \quad \epsilon \to \infty. \tag{3.8}$$

As ν increases from zero it is seen from figure 5 that, before this asymptotic limit is approached, Im F is significantly less than zero in a progressively increasing number of distinct intervals of ϵ. Moreover, the peak values attained by $-\mathrm{Im}\,F$ in these intervals can be very much larger than for $\nu = 0$. As $\nu \to 1$ (vanishing mean shear) the ratio (2.28) defining $F(\epsilon)$ becomes indeterminate, since $\epsilon_1 \to \epsilon_2$, $\sigma_+ \to \sigma_-$. Resolving the indeterminacy by means of l'Hospital's rule we find

$$F(\epsilon) = (\epsilon^2\Delta_0)^{-1}[\![J_0^2+\epsilon^2\{H_0^{(1)}(\sigma)/\mathscr{F}_0\}[(1/\sigma-1/\epsilon)\{J_0^2-\mathrm{i}\epsilon(J_0^2+J_1^2)\}-(J_0/\epsilon)(J_0-\mathrm{i}J_1)]]\!], \quad (3.9)$$

where

$$\Delta_0 = J_1[J_1-\epsilon\{H_1^{(1)}(\sigma)/\mathscr{F}_0\}(J_0-\mathrm{i}J_1)]+(J_0-J_1/\epsilon)[J_0-\epsilon\{H_0^{(1)}(\sigma)/\mathscr{F}_0\}(J_0-\mathrm{i}J_1)]$$
$$+\{H_0^{(1)}(\sigma)J_1-H_1^{(1)}(\sigma)J_0\}\{J_0-\mathrm{i}\epsilon(J_0-\mathrm{i}J_1)\}/\mathscr{F}_0, \quad (3.10)$$

$$\mathscr{F}_0 = \sigma\{H_0^{(1)}(\sigma)-\mathrm{i}H_1^{(1)}(\sigma)\}, \quad (3.11)$$

in which we have set $$J_{0,1} = J_{0,1}(\epsilon), \quad \sigma = \sigma_+ = \sigma_-. \quad (3.12)$$

The arguments of the Bessel and Hankel functions in these expressions are *real*, which implies that when ϵ is large, $F(\epsilon)$ is ultimately the periodic function

$$F(\epsilon) = -(\tfrac{1}{2}+\mathrm{i}e^{2\mathrm{i}\epsilon})/(\tfrac{5}{4}-\sin 2\epsilon). \quad (3.13)$$

The period is equal to π, and the limiting behaviour is already evident in figure 5*f*. Thus, for $\nu = 1$ there exists an infinite sequence of intervals within which Im $F < 0$, and where acoustic energy is extracted from the mean flow. This conclusion is particularly interesting, since it implies that an energy transfer can occur in the absence of instability waves. Indeed, when Im $F < 0$ a net gain of acoustic energy occurs because that generated during the ejection of vorticity at the trailing edge B of the slot exceeds that dissipated at the leading edge A by the shedding of vorticity into the mean flow. This interpretation accords with the predictions of related model problems reported by Howe (1981*b*, §§4, 5).

Self-sustained cavity oscillations

The theory developed in I in the absence of displacement thickness fluctuations was applied to the problem of self-sustained acoustic oscillations of a deep cavity in a wall in the presence of a nominally steady, mean grazing flow. The configuration is illustrated in figure 7, in which a cylindrical cavity of depth l has rectangular cross-section of dimensions $d \times h$ ($l \gg d, h$), and communicates with the ambient medium through a slot of length d and width $2s$ ($s \ll d$). The principal axis of the slot is at right angles to a mean flow of speed U ($\equiv U_+$). Approximate expressions for the coefficients $a_\pm$ that occur in the definitions (2.15) of the Green functions $G_\pm$ were obtained in I by assuming that the perturbed flow in the vicinity of the slot can be regarded as two-dimensional (i.e. uniform in the direction of the x_3-axis).

Depth-mode oscillations within the cavity (which is equivalent to an organ pipe open at *one* end only) have radian frequencies ω_n given approximately by

$$\omega_n = (n-\tfrac{1}{2})\pi c/l \quad (n = 1, 2, \ldots). \quad (3.14)$$

These oscillations are attenuated by the radiation of sound into the ambient medium and through viscous and thermal action in the acoustic boundary layers on the cavity walls. In addition, the perturbation of the mean shear layer over the slot by the acoustic flux leads to an exchange of energy between the standing waves within the cavity and the mean flow, and

energy will be extracted from the mean flow if $-\operatorname{Im}\{F(\epsilon_n)\} > 0$, where $\epsilon_n = \omega_n s/U$. Self-sustaining oscillations are possible provided that sufficient energy can be supplied by this means to overcome the various dissipative mechanisms. It is shown in I that this requires

$$\operatorname{Im}\{-F(\epsilon_n)\} > D(n), \tag{3.15}$$

where
$$D(n) = (n-\tfrac{1}{2})\pi d/4l + \tfrac{1}{2}(l/h)^2(1+h/d)\{\pi/(2n-1)lc\}^{\frac{1}{2}}\{\bar{\nu}^{\frac{1}{2}} + (\gamma-1)\bar{\chi}^{\frac{1}{2}}\}, \tag{3.16}$$

in which $\bar{\nu}$, $\bar{\chi}$ respectively denote the kinematic viscosity and the thermometric conductivity of the fluid in the cavity, and γ is the ratio of specific heats. The first term on the right of (3.16) arises from the radiation damping, and the second from the boundary layer losses.

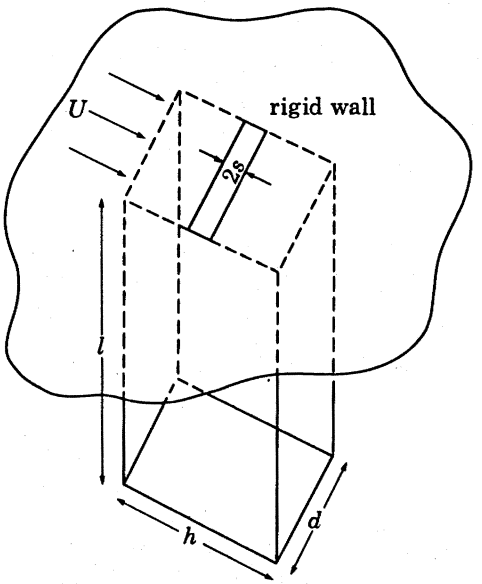

FIGURE 7. Configuration of the wall cavity used in the analysis of self-sustained cavity oscillations.

Since there is no mean flow within the cavity we take $\nu = 0$ in the definition (2.28) of $F(\epsilon)$. Referring to figure 6 we see that in this case $\operatorname{Im} F < 0$ in the range $1 \lesssim \epsilon \lesssim 3$, the precise values of the limits being dependent on the choice of the displacement thickness phase velocity. The behaviour of $\operatorname{Im} F$ in the neighbourhood of the minimum may be specified by the following quadratic approximation:

$$\operatorname{Im}\{F(\epsilon)\} = -A + B(\epsilon - C)^2, \tag{3.17}$$

where the constants A, B, C are positive. By substitution into (3.15) it follows that self-sustained oscillations are possible for Strouhal numbers $\epsilon_n = \omega_n s/U$ that satisfy

$$C - [\{A - D(n)\}/B]^{\frac{1}{2}} < \epsilon_n < C + [\{A - D(n)\}/B]^{\frac{1}{2}}. \tag{3.18}$$

Equivalently, this implies that the nth cavity mode can be excited provided that

$$U_{\min} < U < U_{\max}, \tag{3.19}$$

where
$$\frac{U_{\min}}{c} = \frac{\pi(n-\tfrac{1}{2})(s/l)}{C + [\{A - D(n)\}/B]^{\frac{1}{2}}}; \quad \frac{U_{\max}}{c} = \frac{\pi(n-\tfrac{1}{2})(s/l)}{C - [\{A - D(n)\}/B]^{\frac{1}{2}}}. \tag{3.20}$$

Example

A wall cavity for which $l = 30$ cm, $d = h = 0.2l$, and $s = 1$ cm was considered in I, where vorticity ejection from the cavity was neglected. For air we take $\bar{\nu} = 0.15$ cm^2 s^{-1}, $\bar{\chi} = 0.21$ cm^2 s^{-1}, $\gamma = 1.4$ and $c = 340$ m s^{-1}, in which case

$$D(n) = 0.157(n-\tfrac{1}{2})\{1+0.113/(n-\tfrac{1}{2})^{\frac{3}{2}}\} \quad (n = 1, 2, \ldots). \tag{3.21}$$

The case (i), say, discussed in I corresponds to $\sigma_\pm = \infty$ in (2.28) (no displacement thickness waves), for which we have (cf. figure 6)

$$\text{case (i):} \quad A = 0.31, \quad B = 0.69, \quad C = 2.25. \tag{3.22}$$

When the displacement thickness wave velocity is equal to $0.6U$, so that for $\nu = 0$ we have $\sigma_+ = \frac{5}{3}\epsilon$, $\sigma_- = \infty$, one finds

$$\text{case (ii):} \quad A = 0.72, \quad B \doteq 1.34, \quad C = 2.07. \tag{3.23}$$

The corresponding predicted values of $U_{\min}$, $U_{\max}$ for $n = 1, 2, \ldots$ are given in table 1.

TABLE 1

	case (i), $\sigma_+ = \infty$		case (ii), $\sigma_+ = \frac{5}{3}\epsilon$	
n	$U_{\min}$ / m s^{-1}	$U_{\max}$ / m s^{-1}	$U_{\min}$ / m s^{-1}	$U_{\max}$ / m s^{-1}
1	6.36	10.45	6.48	12.79
2	20.99	27.32	20.06	36.14
3	—	—	34.83	56.19
4	—	—	51.57	72.31
5	—	—	75.15	79.79

In case (i), $D(n) > A$ for $n \geqslant 3$; the corresponding values of $U_{\min}$, $U_{\max}$ are complex, so that such modes cannot be sustained by the mean flow. The corresponding cut-off occurs in case (ii) at $n = 6$. It is apparent that the influence of vorticity ejection is to increase the number of modes that can be excited (by increasing the maximum value of $-\operatorname{Im} F$), and to extend the range of velocities $(U_{\min}, U_{\max})$ over which a particular mode is sustained.

4. The characteristics of the shear layer motion

The formal expression (2.24) for the displacement ζ of the vortex sheet will now be examined in more detail. Making use of the expressions defining $\Theta_0(\chi)$, $\Theta_1(\chi, \xi)$ obtained in the Appendix, one finds that the ratio ζ/Q can be expanded as the Fourier series

$$\frac{\zeta}{Q} = \sum_{n=1}^{\infty} a_n \sin(n\vartheta), \tag{4.1}$$

where $\vartheta = \arccos\xi$ $(0 < \vartheta < \pi)$, and

$$a_n = \frac{2\mathrm{i}^n}{\pi}\left\{\frac{\mathrm{i}\alpha\epsilon_1 J_n(\epsilon_1)}{Q} + \frac{\mathrm{i}\beta\epsilon_2 J_n(\epsilon_2)}{Q} - \frac{h_+(I_n^1 - S_n)\,\mathrm{e}^{\mathrm{i}\sigma_+}}{Q}\right\} \quad (n = 1, 2, \ldots). \tag{4.2}$$

The values of the ratios α/Q, β/Q, h_+/Q are given by equations (A 27) of the Appendix, and I_n^1, S_n are defined by (A 5), (A 22).

It is shown in the Appendix that, when n is large,

$$I_n^1 \simeq \frac{(-\mathrm{i})^n}{n}, \quad S_n \simeq \nu^2 \frac{1-\sigma_-/\sigma_+}{1+\nu^2} \frac{(-\mathrm{i})^n}{n}. \tag{4.3}$$

Since $J_n(z) \simeq (z/2)^n/n!$ for large n, we deduce that, as $n \to \infty$,

$$a_n \simeq \bar{a}_n = \frac{2}{\pi n} \frac{h_+ \mathrm{e}^{\mathrm{i}\sigma_+}}{Q} \frac{1+\nu^2\sigma_-/\sigma_+}{1+\nu^2}. \tag{4.4}$$

This result, that $a_n \simeq O(1/n)$, implies that the series (4.1) does not converge uniformly in $(0, \pi)$, and in particular that ζ/Q does not vanish as $\vartheta \to 0$ ($\xi = +1$) even though every member of the series does. The non-uniformity is avoided by writing

$$\frac{\zeta}{Q} = \sum_{n=1}^{\infty} (a_n - \bar{a}_n) \sin(n\vartheta) + \sum_{n=1}^{\infty} \bar{a}_n \sin(n\vartheta). \tag{4.5}$$

The second series can be summed (Gradshteyn & Ryzhik 1980, p. 38), which leads to

$$\frac{\zeta}{Q} = \frac{h_+ \mathrm{e}^{\mathrm{i}\sigma_+}}{Q} \frac{1+\nu^2\sigma_-/\sigma_+}{1+\nu^2} \left(1 - \frac{\vartheta}{\pi}\right) + \sum_{n=1}^{\infty} (a_n - \bar{a}_n) \sin(n\vartheta). \tag{4.6}$$

In the remaining series the coefficients $a_n - \bar{a}_n \simeq O(1/n^3)$ as $n \to \infty$ (see equation (A 12)), and the sum therefore vanishes at $\vartheta = 0$. Thus at the trailing edge of the slot

$$\begin{aligned} \frac{\zeta}{Q} &= \frac{h_+ \mathrm{e}^{\mathrm{i}\sigma_+}}{Q} \frac{1+\nu^2\sigma_-/\sigma_+}{1+\nu^2} \\ &= \frac{1}{Q} \frac{U_+^2 h_+ \mathrm{e}^{\mathrm{i}\sigma_+} + U_-^2 h_- \mathrm{e}^{\mathrm{i}\sigma_-}}{U_+^2 + U_-^2}. \end{aligned} \tag{4.7}$$

This shows that, when $\sigma_+ = \sigma_-$ (so that $h_+ = h_-$), the displacement ζ of the vortex sheet at the trailing edge of the slot merges continuously with the boundary layer displacement thickness perturbations. In general, however, the displacement is discontinuous at $\zeta = 1$, and the limiting value of the vortex sheet displacement is equal to the average of the boundary layer displacements weighted according to the respective mean dynamic pressures $\rho_0 U_\pm^2$.

The Fourier coefficients $(a_n - \bar{a}_n)$ decay rapidly with increasing values of n, and equation (4.6) may readily be used to compute the displacement of the vortex sheet. We shall compare this with the displacement predicted in the absence of displacement thickness waves. The latter may be obtained by interpreting (4.1) as a generalized function, and taking the formal limit $\sigma_\pm \to \infty$ in the definition (4.2) of the Fourier coefficients a_n. Equations (A 11), (A 24) of the Appendix imply that

$$\left.\begin{aligned} I_n^1 &\simeq (-\mathrm{i})^n (\pi\mathrm{i}/2\sigma_+)^{\frac{1}{2}}, \\ S_n &\simeq (-\mathrm{i})^n \{\nu^2/(1+\nu^2)\}\{(\pi\mathrm{i}/2\sigma_+)^{\frac{1}{2}} - (\sigma_-/\sigma_+)(\pi\mathrm{i}/2\sigma_-)^{\frac{1}{2}}\}, \end{aligned}\right\} \tag{4.8}$$

as $\sigma_\pm \to \infty$, and the corresponding contributions to the Fourier series (4.1) accordingly involve the (generalized) sum

$$\sum_{n=1}^{\infty} \sin(n\vartheta) = \frac{\sin(\vartheta)}{2\{1-\cos(\vartheta)\}} \equiv \frac{1+\xi}{2(1-\xi^2)^{\frac{1}{2}}}. \tag{4.9}$$

The singularity in this result at $\xi = 1$ occurs because the asymptotic forms (4.8) are actually valid only for $\sigma_\pm \gg n$, and their use is tantamount to discarding the tail end of the infinite

series (4.1). When $\sigma_\pm$ are large the influence of the displacement thickness waves is confined to the tail, which makes a non-trivial contribution only in the immediate neighbourhood of the trailing edge of the slot.

Using (4.8) and (4.9) in (4.1), and taking the limiting values of α/Q, β/Q and h_+/Q (in equations (A 27)), we obtain, as $\sigma_\pm \to \infty$,

$$\frac{\zeta}{q} = \frac{1}{\pi(1-\xi^2)^{\frac{1}{2}}}\left[\left[1+\frac{\mathrm{i}S(\epsilon_1)}{\Delta_\infty}\left[J_0(\epsilon_2)-2\mathrm{i}\epsilon_2\{J_0(\epsilon_2)-\mathrm{i}J_1(\epsilon_2)\}\right]-\frac{\mathrm{i}S(\epsilon_2)}{\Delta_\infty}\left[J_0(\epsilon_1)-2\mathrm{i}\epsilon_1\{J_0(\epsilon_1)-\mathrm{i}J_1(\epsilon_1)\}\right]\right]\right], \tag{4.10}$$

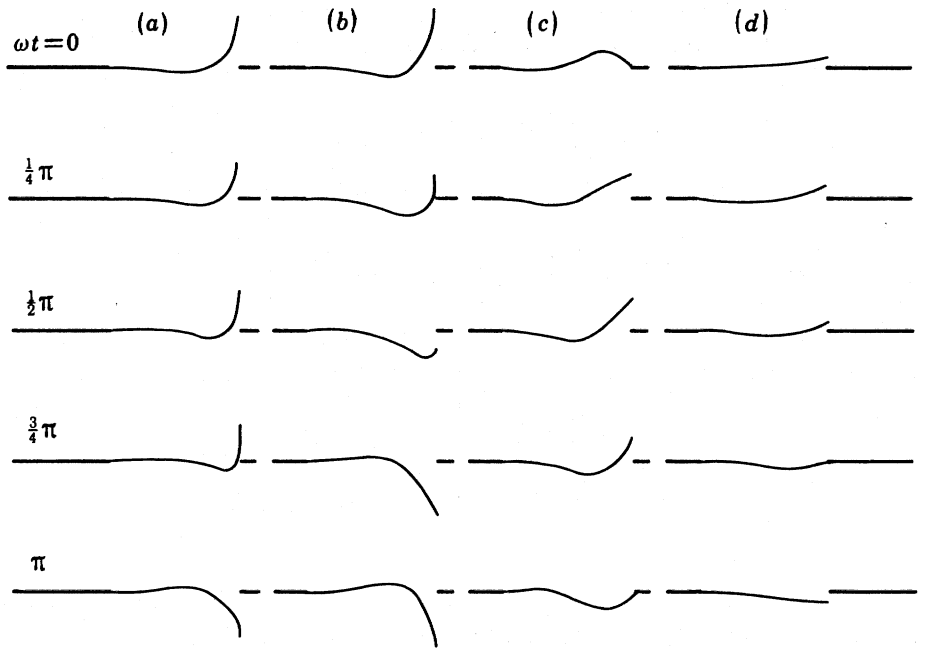

FIGURE 8. Predicted displacements of the vortex sheet for $\epsilon = 2.3$ and for different values of the phase ωt. The mean flow is from left to right: (*a*) equation (4.10) with $\nu = 0$ (no displacement thickness waves); (*b*) equation (4.6) with $\nu = 0$, $\sigma_+ = 5\epsilon/3$, $\sigma_- = \infty$; (*c*) equation (4.6) with $\nu = 0.5$, $\sigma_+ = 5\epsilon/3$, $\sigma_- = 5\epsilon/3\nu$; (*d*) equation (4.6) with $\nu = 1$, $\sigma_\pm = 5\epsilon/3$.

where

$$\Delta_\infty = J_0(\epsilon_2)J_1(\epsilon_1) - J_0(\epsilon_1)J_1(\epsilon_2) + 2(\epsilon_2-\epsilon_1)\{J_0(\epsilon_1)-\mathrm{i}J_1(\epsilon_1)\}\{J_0(\epsilon_2)-\mathrm{i}J_1(\epsilon_2)\}, \tag{4.11}$$

$$S(z) = \xi J_0(z) + \mathrm{i}J_1(z) - 2\sin(\vartheta)\sum_{n=1}^{\infty}\mathrm{i}^n\sin(n\vartheta)J_n(z), \tag{4.12}$$

and it has been noted that $Q \to q$ as $\sigma_\pm \to \infty$ (see equation (4.14)). Equation (4.10) coincides with the analogous result of I which neglects at the outset the influence of the displacement thickness fluctuations.

We illustrate the vortex sheet profiles predicted by these results by a consideration of the particular case $\epsilon = \omega s/U_+ = 2.3$. This is close to the value of ϵ at which $-\mathrm{Im}\,F$ attains its maximum value when $\nu = 0$ and when displacement thickness waves are neglected (cf. figure 4). Equation (4.10) has been used to plot $\mathrm{Re}\{(\zeta/q)\,\mathrm{e}^{-\mathrm{i}\omega t}\}$ in this case (figure 8*a*) at intervals of the phase ωt equal to $\frac{1}{4}\pi$ in $0 \leqslant \omega t \leqslant \pi$. The waveform during the second half-cycle $\pi \leqslant \omega t \leqslant 2\pi$ is obtained by inverting the profile at time π/ω earlier. At $\xi = 1$, $\zeta \to \infty$ like $(1-\xi)^{-\frac{1}{2}}$.

Figures 8*b–d* depict the corresponding profiles (drawn to the same scale as 8*a*) predicted in the presence of displacement thickness fluctuations by (4.6) for $\nu = 0, 0.5, 1$ respectively, and when the displacement thickness phase velocities are equal to 60% of the mean stream velocity (as in (3.7)). The displacement ζ is finite at $\xi = 1$. For $\nu = 0$, σ_+ is finite, but $\sigma_- = \infty$ and (cf. (4.7)) $\zeta \to h_+ e^{i\sigma_+}$ at $\xi = 1$. Corresponding profiles in figures 8*a*, *b* are seen to be similar except near the trailing edge, where the phase of the latter is a little ahead of the curve for no displacement thickness waves. The figures show that as ν increases to unity (no mean shear) the amplitude of the motion of the vortex sheet is greatly reduced. This result might be expected inasmuch as the vorticity fluctuations within the slot diminish in strength as $\nu \to 1$ Indeed, from a consideration of the incompressible form of the vorticity equation

$$\partial\boldsymbol{\omega}/\partial t = -\operatorname{curl}(\boldsymbol{\omega} \wedge \boldsymbol{v}), \tag{4.13}$$

in which $\boldsymbol{\omega}$ is the vorticity and $\boldsymbol{v}$ the velocity, it is easy to show that, within the slot,

$$\partial\omega_3/\partial t \propto \partial^2\chi(\xi)/\partial\xi^2,$$

where $\chi(\xi)$ is the function defined in (2.20). The terms in α and β on the right of equation (2.20) represent the Kelvin–Helmholtz instability waves, whose growth rates vanish in the absence of mean shear ($\nu \to 1$).

Relation between the shear layer flux q and the trailing edge flux q_h

In the absence of the ejection of vorticity from the slot the net flux Q is equal to q, that produced by the motion of the vortex sheet. When displacement thickness fluctuations are taken into account, $Q = q + q_h$ is shared between q and the component $q_h = ih_\pm e^{i\sigma_\pm}/\sigma_\pm$ at the trailing edge of the slot. Equations (A 27) of the Appendix may be used to show that the fractional flux through the end of the slot is given by

$$\begin{aligned} q_h/Q &= \{2ie^{i\sigma_+}/(\pi\sigma_+\Delta\mathscr{F})\}[\epsilon_1 J_0(\epsilon_2)\{J_0(\epsilon_1) - iJ_1(\epsilon_1)\} - \epsilon_2 J_0(\epsilon_1)\{J_0(\epsilon_2) - iJ_1(\epsilon_2)\}] \\ &\equiv \Psi(\epsilon), \quad \text{say,} \end{aligned} \tag{4.14}$$

where Δ, $\mathscr{F}$ are defined by equations (2.29)–(2.32). As $\sigma_\pm \to \infty$ it follows from these equations that Δ remains finite and non-zero, and $\mathscr{F} \simeq O(1/\sigma_+^{\frac{1}{2}})$. This implies that $q_h/Q \simeq O(1/\sigma_+^{\frac{1}{2}})$, and that the trailing edge component of the flux ultimately vanishes.

Rearranging (4.14), we have

$$q_h/q = \Psi(\epsilon)/\{1 - \Psi(\epsilon)\}. \tag{4.15}$$

The variations of the real and imaginary parts of q_h/q as functions of ϵ, for $\nu = 0, 0.5, 1$, are illustrated in figure 9. As before, it is assumed that $\sigma_\pm = 5\omega s/3U_\pm$. When ϵ is large one finds from (4.15) that

$$q_h/q \simeq -1 + O(1/\epsilon^{\frac{1}{2}}). \tag{4.16}$$

This general behaviour is apparent in figures 9*a*, *b*. When $\nu = 1$,

$$q_h/q \simeq -1 + (1 - 2ie^{-2i\epsilon})(i\pi\sigma/8\epsilon^2)^{\frac{1}{2}} \quad (\sigma = \sigma_\pm), \tag{4.17}$$

and the asymptotic limit is approached slowly. It is evident that at high values of the Strouhal number ϵ, the net flux Q arises from a delicate imbalance between opposing fluxes q of the vortex sheet and q_h at the trailing edge. The magnitude of Q amounts to a small fraction of either of these quantities:

$$Q \simeq O(q/\epsilon^{\frac{1}{2}}). \tag{4.18}$$

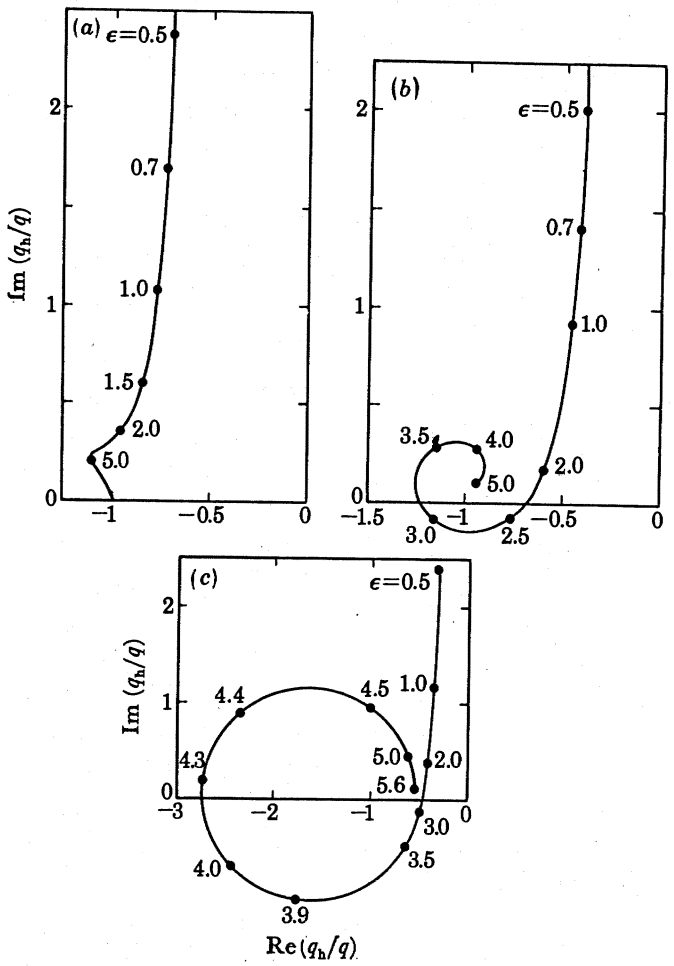

FIGURE 9. Dependence of q_h/q on the Strouhal number $\epsilon = \omega s/U_+$: (*a*) $\nu = 0$; (*b*) $\nu = 0.5$; (*c*) $\nu = 1$.

5. THE CASE OF NO MEAN SHEAR: DIFFRACTION BY A PERFORATED SCREEN IN GRAZING FLOW

Unsteady motion in a slot in the absence of mean shear has been examined by Howe (1980) in connection with the diffraction of sound by a screen perforated with an array of parallel, equal and equidistant slots (see figure 10). Let $v(\xi)$ denote the x_2-component of the perturbation velocity within the slot. Setting $U = U_\pm$, we have

$$v(\xi) = -\mathrm{i}U(\epsilon + \mathrm{i}\partial/\partial\xi)\,\zeta \quad (|\xi| < 1). \tag{5.1}$$

Howe (1980) took no account of the possibility of the ejection of vorticity from the slot, and derived the following formula:

$$v(\xi) = \frac{-\mathrm{i}q\omega s}{\pi(1-\xi^2)^{\frac{1}{2}}}\left\{(1+\xi)J_0(\epsilon) - 2\sin\vartheta\sum_{n=1}^{\infty}\mathrm{i}^n\sin(n\vartheta)J_n(\epsilon)\right\}\Big/\{J_0(\epsilon)-\mathrm{i}J_1(\epsilon)\} \quad (|\xi| < 1), \tag{5.2}$$

where, as above, $\vartheta = \arccos\xi$, and q is the flux defined as in (2.14).

Equation (5.2) satisfies the Kutta condition that $v(\xi) \to 0$ at the leading edge of the slot; at the trailing edge $v(\xi) \simeq O\{1/(1-\xi)^{\frac{1}{2}}\}$. The flux q is related to the incident acoustic pressure p_0 by an equation of the form (2.27) in which $F(\epsilon)$ is replaced by

$$F_0(\epsilon) = (\mathrm{i}/\epsilon)\, J_0(\epsilon)/\{J_0(\epsilon) - \mathrm{i}J_1(\epsilon)\} \quad (\epsilon > 0). \tag{5.3}$$

Im F_0 is positive for $\epsilon > 0$, which implies that acoustic energy is always *absorbed* at the slot. This energy is expended in the formation of vorticity at the leading edge of the slot. The vortex elements occupy a vortex sheet and are swept downstream by the mean flow. It was tacitly assumed by Howe (1980) that the vorticity is annulled by image vortices in the plate on arrival at the trailing edge B of the slot (see figure 2).

The conclusions of Howe (1980) are at variance with the theory of the present paper. The appropriate comparison is with the case in which $\nu = 1$ and $\sigma_\pm \to \infty$ in the formulae of §§2–4, which corresponds to an absence of mean shear and displacement thickness fluctuations. In particular, letting $\sigma \to \infty$ in (3.9), we have, instead of (5.3),

$$F(\epsilon) = \frac{-1}{\epsilon}\left[\frac{\{J_0 - 2\mathrm{i}\epsilon(J_0 - \mathrm{i}J_1)\}\{J_0 - \mathrm{i}\epsilon(J_0 + \mathrm{i}J_1)\} - \mathrm{i}\epsilon J_0(J_0 - \mathrm{i}J_1)}{J_0 J_1 + \epsilon\{J_1^2 + (J_0 - 2\mathrm{i}J_1)^2\}}\right], \tag{5.4}$$

where $J_{0,1} = J_{0,1}(\epsilon)$. Similarly, although $v(\xi)$ vanishes at the leading edge of the slot, we now have $v \simeq O(1/(1-\xi)^{\frac{3}{2}})$ at $\xi = 1$. The inverse square root singularity of Howe (1980) is obtained only when $\sigma_\pm$ are finite, i.e. in the presence of displacement thickness waves. Such waves are generated by slot vorticity in the immediate vicinity of the trailing edge. We here claim that a proper modelling of the motion must take account of these boundary layer disturbances, and that the analysis given by Howe (1980) is inconsistent with his hypothesis that slot vorticity is cancelled by images at the trailing edge. To be sure, cancellation is possible only if the displacement of the vortex sheet *vanishes* at the trailing edge. That this is not the case can be deduced by integrating (5.1) and introducing (5.2) to obtain

$$\begin{aligned}\zeta(1) &= \frac{\mathrm{e}^{\mathrm{i}\epsilon}}{U}\int_{-1}^{1} v(\xi)\,\mathrm{e}^{-\mathrm{i}\epsilon\xi}\,\mathrm{d}\xi \\ &= -\frac{\mathrm{i}q\epsilon\,\mathrm{e}^{\mathrm{i}\epsilon}}{J_0 - \mathrm{i}J_1}\left\{J_0(J_0 - \mathrm{i}J_1) - \frac{2\mathrm{i}}{\epsilon}\sum_{n=1}^{\infty} nJ_n^2\right\},\end{aligned} \tag{5.5}$$

in which $J_n = J_n(\epsilon)$. The infinite series is summed by using the relation

$$J_n^2(\epsilon) = \frac{2}{\pi}\int_0^{\frac{1}{2}\pi} J_{2n}(2\epsilon\cos\theta)\,\mathrm{d}\theta,$$

and a summation formula given by Gradshteyn & Ryzhik (1980, pp. 738, 974), so that finally

$$\zeta(1) = -\mathrm{i}q\epsilon\,\mathrm{e}^{\mathrm{i}\epsilon}\{J_0^2 - \mathrm{i}\epsilon(J_0^2 + J_1^2)\}/(J_0 - \mathrm{i}J_1). \tag{5.6}$$

The term of this result in the curly brackets is non-zero for arbitrary positive ϵ, indicating that $\zeta(1)$ vanishes only if $q = 0$, i.e. in the absence of acoustic fluctuations.

Attenuation of sound by a perforated screen

The remainder of this section summarizes the extent to which the theory of the present paper modifies the conclusions of Howe (1980).

The parallel slots in the screen (see figure 10) are equally spaced with periodic distance d; A_0 denotes the fractional open area of the screen:

$$A_0 = 2s/d. \tag{5.7}$$

A plane sound wave is incident on the screen from $x_2 > 0$, and is specified by the polar angles (θ, ϕ) $(0 \leqslant \theta \leqslant \frac{1}{2}\pi, 0 \leqslant \phi \leqslant 2\pi)$ which define the direction of the *wave-normal* (i.e. the normal to the surfaces of constant phase), θ being the angle of incidence measured from the positive direction of the x_2-axis, and ϕ being measured from the x_1-direction.

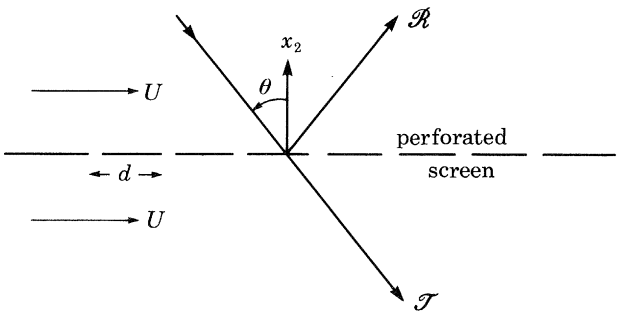

FIGURE 10. Diffraction of sound by a perforated screen in a uniform grazing mean flow.

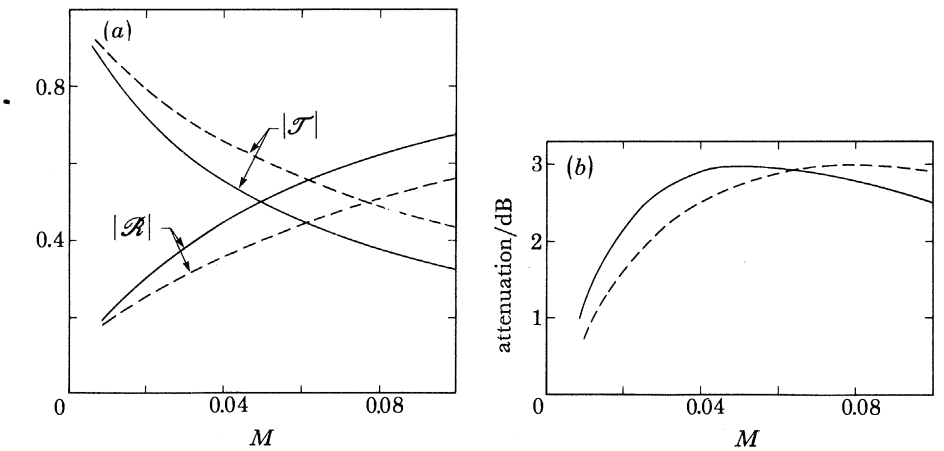

FIGURE 11. Dependence of (*a*) $|\mathscr{R}|$, $|\mathscr{T}|$ and (*b*) the attenuation on the grazing flow Mach number for a normally incident sound wave and for $kd = 0.3$, $A_0 = 0.05$. ——, Theory of this paper; – – –, theory of Howe (1980).

Reflexion and transmission coefficients respectively denoted by $\mathscr{R}, \mathscr{T}$ are given by

$$\mathscr{T} = 1 - \mathscr{R} = 1/(1 + \bar{\gamma} + \mathrm{i}\bar{\delta}), \tag{5.8}$$

in which

$$\left.\begin{aligned} \bar{\gamma} &= \{kd \cos\theta/(1 + M \sin\theta \cos\phi)\} \operatorname{Im}\{F(\epsilon)\}, \\ \bar{\delta} &= \{-kd \cos\theta/(1 + M \sin\theta \cos\phi)\} [\ln(2/\pi A_0) + \operatorname{Re}\{F(\epsilon)\}]. \end{aligned}\right\} \tag{5.9}$$

In deriving these formulae it is assumed that $kd = \omega d/c \ll 1$. Recall that $F(\epsilon)$ was calculated in §2 on the assumption that displacement thickness waves *incident* on a slot are uncorrelated with the acoustic flux through the slot. Such waves are, in fact, produced by other, upstream slots, and their neglect in the evaluation of (5.9) may be justified by noting that in practice (i) disturbances translating in a turbulent boundary layer rapidly lose their coherence and

(ii) a real screen is likely to be perforated with *circular* apertures with $A_0 \lesssim 0.05$, and the probability that an aperture lies in the wake of an upstream, neighbouring aperture is therefore very small.

The Strouhal number ϵ is related to the Mach number M of the grazing mean flow by

$$\epsilon = \omega s/U \equiv (kd/2M)\,A_0. \tag{5.10}$$

This can be used in equation (3.9) (for which $\nu = 1$) to determine $F(\epsilon)$ as a function of M for a fixed value of the acoustic wavenumber k. The solid curves in figure 11*a* indicate the dependence of $\mathscr{R}$ and $\mathscr{T}$ on M for a sound wave incident normally on the screen, for $kd = 0.3$, $A_0 = 0.05$, and when the displacement thickness wave velocity is equal to $0.6U$ ($\sigma = \sigma_{\pm} = 5\epsilon/3$). The dashed curves represent the corresponding predictions of Howe (1980), which can be obtained from (5.9) by using equation (5.3). The corresponding attenuations of the sound at the screen (in decibels) are compared in figure 11*b*. The attenuation is equal to $-10 \lg \bar{\Delta}$, where

$$\bar{\Delta} = |\mathscr{R}|^2 + |\mathscr{T}|^2, \tag{5.11}$$

which is the ratio of the sum of the transmitted and reflected acoustic intensities to that of the incident wave.

According to figure 11 the predictions of the two theories are unlikely to be significantly different in practice. The nature of the differences may be examined in more detail by noting, from (5.10), that ϵ is usually small except when M is very small (for example, for the parametric values used above, ϵ decreases rapidly from 0.5 when M exceeds 0.015). For small ϵ we find from (3.9) and (5.3):

$$F(\epsilon) \simeq \mathrm{i}\sigma/\epsilon^2; \quad F_0(\epsilon) \simeq \mathrm{i}/\epsilon. \tag{5.12}$$

Thus, at low Strouhal numbers the theories would agree if the phase velocity of the displacement thickness disturbances were equal to that of the ambient mean flow, and it is this that accounts for the differences illustrated in figure 11.

Equations (5.9) and the first of (5.12) may be used to show that when kd is very small

$$\bar{\Delta} \simeq (1 + \Omega^2 \cos^2\theta)/(1 + \Omega\cos\theta)^2, \tag{5.13}$$

where $\Omega = 2M/\pi A_0 V$ and $V = \epsilon/\sigma$ is the fractional phase velocity of the displacement thickness waves. It may be verified that (5.13) is within 5% of the curves shown in figure 11*b* when $M \gtrsim 0.02$. Perforated screens are deployed in heat exchanger cavities to attenuate aerodynamically generated sound, and this approximate formula may be applied to estimate the value of Ω that optimizes this attenuation. To do this (5.13) is averaged over all equally probable directions (θ, ϕ) of the incident sound, yielding

$$\langle\bar{\Delta}\rangle = \int_0^{\frac{1}{2}\pi} \bar{\Delta}(\theta)\sin\theta\,\mathrm{d}\theta = \frac{3+\Omega}{1+\Omega} - \frac{2}{\Omega}\ln(1+\Omega). \tag{5.14}$$

This attains a minimum value of 0.57 (giving an attenuation of 2.46 dB) at $\Omega = 2.16$. However, $\langle\bar{\Delta}\rangle$ varies very slowly in the neighbourhood of this point, being within 10% of the minimum for $1 < \Omega < 5$. Any value of Ω in this range will be suitable in practice, which indicates that the uncertainty in the precise value of the fractional phase velocity V (and its variation with ϵ) is not important.

6. Comparison with experiment

Ronneberger (1980) has used a photographic technique to obtain detailed measurements of the displacement of a thin shear layer formed by laminar grazing flow over a rectangular cut-out in a plate that spans the test section of a water tunnel (see figure 12). The shear layer was driven by a piston within the cavity, and was made visible by means of dye injected into the flow upstream of the cavity. The cavity width, $2s$, was 4 cm, and the span was equal to 25 cm. The mean flow velocity U ($\equiv U_+$) was equal to 12.3 or 13.1 cm s^{-1} with corresponding values of the momentum thickness δ^* of the boundary layer just upstream of the cavity equal to 0.134, 0.08 cm. Thus $2s/\delta^* \gg 1$, and this would appear to justify the vortex sheet approximation to the shear layer.

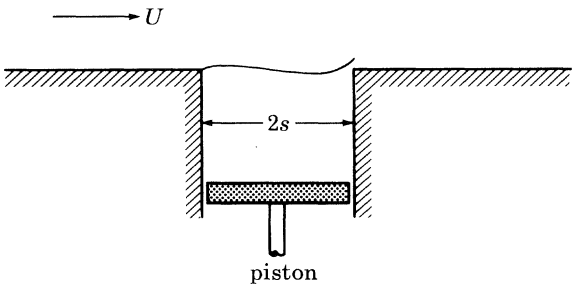

Figure 12. Schematic illustration of Ronneberger's (1980) experiment.

Table 2

case	$\epsilon = \omega s/U$	U / cm s^{-1}	Re $\bar{\epsilon}_2$	Im $\bar{\epsilon}_2$
I	0.70	13.1	1.00	−0.90
II	2.10	13.1	4.24	−1.48
III	3.45	12.3	6.19	−2.22

Table 2 lists data taken from Ronneberger's paper for three typical experimental cases. The last two columns represent Ronneberger's experimental determination of the real and imaginary parts of the wavenumber $\bar{\epsilon}_2$ of the instability wave on the shear layer, which, in principle, corresponds to ϵ_2 of equations (2.22).

Case I

Since there is no mean flow within the cavity, we take $\nu = 0$, $\epsilon = 0.70$ in (2.22), obtaining $\epsilon_2 = 0.7(1-\mathrm{i})$. Thus, although the real and imaginary parts of $\bar{\epsilon}_2$ have approximately the same magnitudes, they are about 40% greater than the analogous components predicted for a vortex sheet at the same Strouhal number. Ronneberger measured the displacement Z of the shear layer at selected values of ξ ($|\xi| < 1$). The results were normalized with respect to the (complex) displacement h_0, say, of the piston, and the logarithmic amplitude $\ln|Z/h_0|$ and the phase $\arg(Z/h_0)$ were plotted as illustrated by the experimental points in figure 13.

To obtain a comparison with the theory we first observe that differences must be expected simply because of the different geometrical configurations (sharp-edged slot of the theory as opposed to the square-edged cavity of the experiments). These differences would be expected to be significant precisely when the influence of displacement thickness waves is important,

since a rigid boundary is equivalent to a distribution of unsteady vorticity. Accordingly two comparisons are made below: the first neglects displacement thickness waves and uses (4.10) to calculate ζ/q; the second uses (4.6) to determine ζ/Q when $\sigma_+ = \sigma_- = \frac{5}{3}\epsilon$. The assumption that σ_- is finite in the second comparison is intended to model the sweeping away of vorticity by the mean flow which enters the cavity near the trailing edge. Note that the motion within the cavity may be taken to be incompressible, and Z/h_0 is therefore equal to $2\zeta/Q$, $2\zeta/q$ according as equation (4.6) or (4.10) is being used.

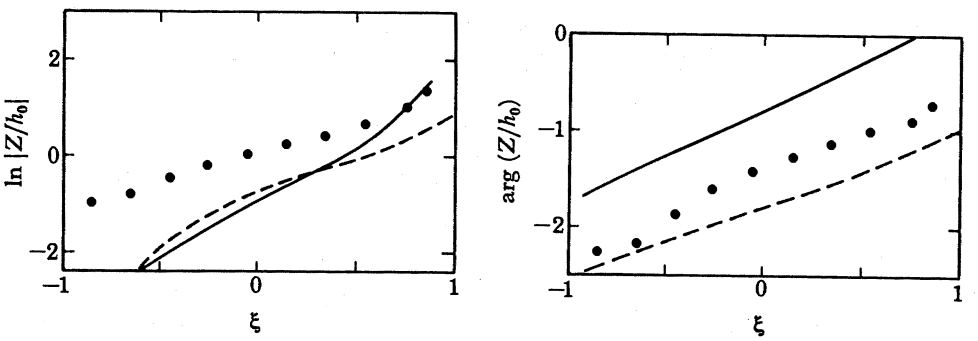

FIGURE 13. Comparison of theory and experiment, case I of table 2: ●●●, experiment (Ronneberger 1980); ——, theory, no displacement thickness waves; – – –, theory, with displacement thickness waves.

The solid and dashed curves in figure 13 respectively represent the vortex sheet displacement calculated without or with displacement thickness waves for $\nu = 0$ and $\epsilon = 0.70$. In both cases the predicted phase curves exhibit an almost linear dependence on ξ, corresponding to a propagating wave, and closely parallel the experimental points. The discrepancy in the amplitude between theory and experiment is large, and can probably be attributed to the influence of cavity geometry. At the relatively low Strouhal number of 0.7 the hydrodynamic wavelength of the motion $2\pi s/\epsilon \approx 9s$ is large compared with the width of the cavity. The vortex sheet is therefore likely to be strongly coupled over the whole of its length to the image vortices in the walls of the cavity.

Cases II, III

The Strouhal numbers are here sufficiently large that edge effects may be expected to be of much less significance. Reference to table 2, however, reveals that the magnitudes of the real and imaginary parts of $\bar{\epsilon}_2$ are decidedly unequal, indicating that a vortex sheet provides a totally inadequate model of the shear layer. Ronneberger has shown that the values of $\bar{\epsilon}_2$ quoted in table 2 are in excellent agreement with the eigenvalue predictions made by Michalke (1965) for an inviscid shear layer with a hyperbolic-tangent velocity profile. This suggests that a comparison of experiment with the vortex sheet theory is still possible provided the values of the wavenumbers $\epsilon_{1,2}$ of the instability waves are adjusted to coincide with those of a shear layer of finite width. We can do this by equating ϵ_2 and $\bar{\epsilon}_2$ using table 2, which is equivalent to assigning the effective values given in table 3 to ϵ and ν. We shall continue to assume that, when present, the displacement thickness waves have phase velocity equal to 60% of the mean stream velocity U. This requires that $\sigma_\pm = \frac{5}{3}\epsilon$, where ϵ takes the values listed in table 2 for cases II and III.

The solid and dashed curves in figures 14 and 15 represent the theoretical prediction obtained as described above without and with displacement thickness waves for cases II and III respectively In the absence of displacement thickness fluctuations both figures exhibit remarkable agreement in amplitude between theory and experiment. The agreement in phase is not as impressive, however, although the respective experimental and theoretical net changes in phase across the cavity are equal.

TABLE 3

case	effective values ϵ	ν
II	3.53	0.48
III	5.14	0.47

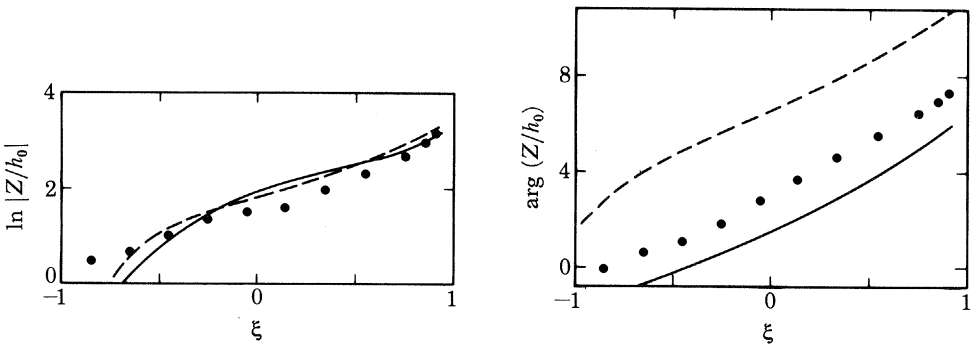

FIGURE 14. As for figure 13 for case II of table 2.

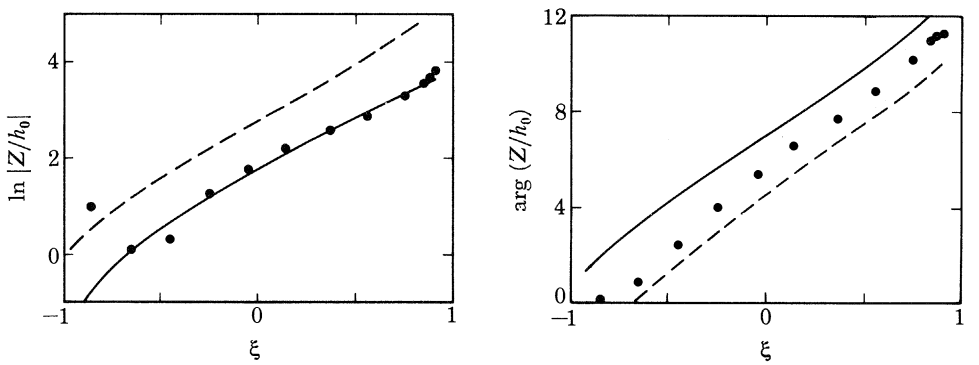

FIGURE 15. As for figure 13 for case III of table 2.

It might be thought paradoxical that the predicted phase should differ from experiment when there is effective agreement in amplitude, inasmuch as this appears to violate continuity of matter within the cavity. But it is readily verified that the terms involving $S(\epsilon_1)$, $S(\epsilon_2)$ in the open square brackets of (4.10) actually make no contribution to the net flux; the latter arises from the first term (unity) which is always in phase with the motion of the piston (i.e. with q) and, except near the edges of the cavity, corresponds to a logarithmic amplitude $\ln|Z/h_0| \approx -0.45$. This is much smaller than the measured and predicted amplitudes of figures 14 and 15 and implies that the large-amplitude excursions of the shear layer are not, in fact, associated with a net flux through the slot.

PHILOSOPHICAL TRANSACTIONS OF THE ROYAL SOCIETY A MATHEMATICAL, PHYSICAL & ENGINEERING SCIENCES

to $-\mathrm{i}\infty$ by recalling (Gradshteyn & Ryzhik 1980, p. 968) that the values of $H_n^{(2)}$ on the upper and lower sides of the branch cut are related by

$$H_n^{(2)}(k\,\mathrm{e}^{2\pi\mathrm{i}}) = H_n^{(2)}(k) + 4J_n(k). \tag{A 7}$$

Use of this in (A 6) yields

$$\left.\begin{aligned} I_0^j &= \tfrac{1}{2}\pi\mathrm{i}H_0^{(1)}(\sigma_j)\,\mathrm{e}^{-\mathrm{i}\sigma_j}, \\ I_1^j &= \tfrac{1}{2}\pi\mathrm{i}H_1^{(1)}(\sigma_j)\,\mathrm{e}^{-\mathrm{i}\sigma_j} - 1/\sigma_j. \end{aligned}\right\} \tag{A 8}$$

For $n \geqslant 2$ the following recurrence relation is easily derived from the definition (A 5):

$$I_n^j = 2(n-1)\,I_{n-1}^j/\sigma_j - I_{n-2}^j - 2(-\mathrm{i})^{n-1}/\sigma_j. \tag{A 9}$$

When $|\sigma_j| \gg n$ it follows from (A 8) and (A 9) that

$$I_n^j \simeq \tfrac{1}{2}\pi\mathrm{i}H_n^{(1)}(\sigma_j)\,\mathrm{e}^{-\mathrm{i}\sigma_j} + O(1/\sigma_j), \tag{A 10}$$

i.e., with the use of the asymptotic form of the Hankel function (Gradshteyn & Ryzhik 1980, p. 962),

$$I_n^j \simeq (-\mathrm{i})^n(\pi\mathrm{i}/2\sigma_j)^{\frac{1}{2}} \quad (|\sigma_j| \gg n, \quad n = 0, 1, 2, \ldots). \tag{A 11}$$

For $n \gg |\sigma_j|$, an asymptotic development of I_n^j follows directly from (A 5):

$$\begin{aligned} I_n^j &\simeq \sum_{m\geqslant 0}\int_0^\infty \frac{(\sigma_j/k)^m}{k}\,J_n(k)\,\mathrm{e}^{-\mathrm{i}k}\,\mathrm{d}k \quad (n \gg m) \\ &= (-\mathrm{i})^n \sum_{m\geqslant 0} \frac{(2\mathrm{i}\sigma_j)^m\,\Gamma(n-m)\,\Gamma(m+\frac{1}{2})}{\pi^{\frac{1}{2}}\Gamma(n+m+1)} \\ &= \frac{(-\mathrm{i})^n}{n}\left\{1 + \frac{\mathrm{i}\sigma_j}{n^2-1} + \frac{1\times 3(\mathrm{i}\sigma_j)^2}{(n^2-1)\,(n^2-2^2)} + \frac{1\times 3\times 5(\mathrm{i}\sigma_j)^3}{(n^2-1)\,(n^2-2^2)\,(n^2-3^2)} + \ldots\right\} \end{aligned} \tag{A 12}$$

(see Gradshteyn & Rzyhik 1980, p. 747).

Evaluation of $\Theta_0(\chi_2)$, $\Theta_1(\chi_2, \xi)$

From Gradshteyn & Rzyhik (1980, pp. 527, 956)

$$\Theta_0(\chi_2) = (\mathrm{i}h_+/\sigma_+)\,\mathrm{e}^{\mathrm{i}\sigma_+}\ln 2 + (\pi h_+/2\sigma_+)\,H_0^{(1)}(\sigma_+). \tag{A 13}$$

Differentiating χ_2 with respect to ξ, and using the alternative integral representation

$$\chi_2'(\xi) = h_+\mathrm{e}^{\mathrm{i}\sigma_+}\int_0^\infty \frac{\mathrm{e}^{\mathrm{i}k(\xi-1)}\mathrm{d}k}{k-\sigma_+} \quad (\mathrm{Im}\,\sigma_+ > 0), \tag{A 14}$$

one finds by analogy with $\Theta_1(\chi_1, \xi)$

$$\Theta_1(\chi_2, \xi) = -h_+\mathrm{e}^{\mathrm{i}\sigma_+}\int_0^\infty \frac{\mathrm{e}^{-\mathrm{i}k}}{k-\sigma_+}\left\{\xi J_0(k) + \mathrm{i}J_1(k) - 2\sin\vartheta\sum_{n=1}^\infty \mathrm{i}^n\sin(n\vartheta)\,J_n(k)\right\}\mathrm{d}k, \tag{A 15}$$

i.e. by (A 5), with $j = 1$,

$$\Theta_1(\chi_2, \xi) = -h_+\mathrm{e}^{\mathrm{i}\sigma_+}\left\{\xi I_0^1 + \mathrm{i}I_1^1 - 2\sin\vartheta\sum_{n=1}^\infty \mathrm{i}^n\sin(n\vartheta)\,I_n^1\right\}. \tag{A 16}$$

Evaluation of $\Theta_0(\chi_3)$, $\Theta_1(\chi_3, \xi)$

By analogy with $\Theta_0(\chi_1)$, we have

$$\Theta_0(\chi_3) = \mathrm{i}h_+\nu^2\mathrm{e}^{\mathrm{i}\sigma_+}(1-\sigma_-/\sigma_+)\int_0^\infty \frac{(k-\epsilon_-)^2 J_0(k)\,\mathrm{e}^{-\mathrm{i}k}\mathrm{d}k}{f(k)}. \tag{A 17}$$

Resolving the integrand into partial fractions and using the definition (A 5) we obtain

$$\Theta_0(\chi_3) = -\tfrac{1}{2}\pi h_+ \nu^2 (1-\sigma_-/\sigma_+) \sum_{j=1}^{4} \frac{(\sigma_j-\epsilon_-)^2}{f_j'} H_0^{(1)}(\sigma_j)\, \mathrm{e}^{\mathrm{i}(\sigma_+-\sigma_j)}. \tag{A 18}$$

Again, by analogy with $\Theta_1(\chi_1, \xi)$,

$$\Theta_1(\chi_3, \xi) = h_+ \nu^2 \mathrm{e}^{\mathrm{i}\sigma_+}(1-\sigma_-/\sigma_+) \int_0^\infty \frac{k(k-\epsilon_-)^2}{f(k)} \Big\{ \xi J_0(k) + \mathrm{i} J_1(k) - 2\sin(\vartheta) \sum_{n=1}^{\infty} \mathrm{i}^n \sin(n\vartheta) J_n(k) \Big\} \mathrm{e}^{-\mathrm{i}k}\,\mathrm{d}k. \tag{A 19}$$

Introduce the partial fraction decomposition

$$\left.\begin{aligned} \nu^2(1-\sigma_-/\sigma_+)\frac{k(k-\epsilon_-)^2}{f(k)} &= \sum_{j=1}^{4} \frac{A^j}{k-\sigma_j}, \\ A^j &= \nu^2(1-\sigma_-/\sigma_+)\sigma_j(\sigma_j-\epsilon_-)^2/f_j', \end{aligned}\right\} \tag{A 20}$$

in which case (A 19) becomes

$$\Theta_1(\chi_3, \xi) = h_+ \mathrm{e}^{\mathrm{i}\sigma_+} \Big\{ \xi S_0 + \mathrm{i} S_1 - 2\sin(\vartheta) \sum_{n=1}^{\infty} \mathrm{i}^n \sin(n\vartheta) S_n \Big\}, \tag{A 21}$$

where

$$S_n = \sum_{j=1}^{4} A^j I_n^j \quad (n \geqslant 0). \tag{A 22}$$

The following properties of S_n are required:

$$S_n \simeq \frac{(-\mathrm{i})^n}{n} \sum_{j=1}^{4} A^j = \frac{\nu^2(1-\sigma_-/\sigma_+)}{1+\nu^2} \frac{(-\mathrm{i})^n}{n} \tag{A 23}$$

for $n \gg \max|\sigma_j|$.

As $\sigma_1, \sigma_2 \to \infty$ for fixed σ_3, σ_4 (i.e. as $\sigma_\pm \to \infty$), it follows from (A 11), (A 20) that

$$S_n \simeq (-\mathrm{i})^n \sum_{j=1}^{2} A^j (\pi\mathrm{i}/2\sigma_j)^{\frac{1}{2}}, \tag{A 24}$$

where, as $\sigma_\pm \to \infty$,

$$A^1 \to \nu^2/(1+\nu^2), \quad A^2 \to -(\sigma_-/\sigma_+)\nu^2/(1+\nu^2). \tag{A 25}$$

The boundary conditions (2.26)

Collecting together the results derived above one obtains the following, respective explicit forms of equations (2.26*a–d*):

$$Q\{\ln 2 - \tfrac{1}{2}\pi(a_+ + a_-)\} + \alpha J_0(\epsilon_1) + \beta J_0(\epsilon_2) + (\pi h_+/2\sigma_+) H_0^{(1)}(\sigma_+) - \tfrac{1}{2}\pi\nu^2 h_+(1-\sigma_-/\sigma_+) \sum_{j=1}^{4} \frac{(\sigma_j-\epsilon_-)^2}{f_j'} H_0^{(1)}(\sigma_j)\, \mathrm{e}^{\mathrm{i}(\sigma_+-\sigma_j)} = \frac{\pi p_0}{2\rho_0 \epsilon_+^2 U_+^2}; \tag{A 26a}$$

$$Q \pm \mathrm{i}\alpha\epsilon_1\{J_0(\epsilon_1) \mp \mathrm{i}J_1(\epsilon_1)\} \pm \mathrm{i}\beta\epsilon_2\{J_0(\epsilon_2) \mp \mathrm{i}J_1(\epsilon_2)\} \pm \tfrac{1}{2}\mathrm{i}\pi h_+\{H_0^{(1)}(\sigma_+) \mp \mathrm{i}H_1^{(1)}(\sigma_+)\} \mp \tfrac{1}{2}\mathrm{i}\pi\nu^2 h_+(1-\sigma_-/\sigma_+) \sum_{j=1}^{4} \frac{\sigma_j(\sigma_j-\epsilon_-)^2}{f_j'} [H_0^{(1)}(\sigma_j) \mp \mathrm{i}H_1^{(1)}(\sigma_j)]\, \mathrm{e}^{\mathrm{i}(\sigma_+-\sigma_j)} = 0; \tag{A 26b, c}$$

$$\alpha\epsilon_1[J_0(\epsilon_1) - 2\mathrm{i}\epsilon_1\{J_0(\epsilon_1) - \mathrm{i}J_1(\epsilon_1)\}] + \beta\epsilon_2[J_0(\epsilon_2) - 2\mathrm{i}\epsilon_2\{J_0(\epsilon_2) - \mathrm{i}J_1(\epsilon_2)\}] + \tfrac{1}{2}\pi h_+[H_0^{(1)}(\sigma_+) - 2\mathrm{i}\sigma_+\{H_0^{(1)}(\sigma_+) - \mathrm{i}H_1^{(1)}(\sigma_+)\}] - \tfrac{1}{2}\pi\nu^2 h_+(1-\sigma_-/\sigma_+) \sum_{j=1}^{4} \frac{\sigma_j(\sigma_j-\epsilon_-)^2}{f_j'} [H_0^{(1)}(\sigma_j) - 2\mathrm{i}\sigma_j\{H_0^{(1)}(\sigma_j) - \mathrm{i}H_1^{(1)}(\sigma_j)\}]\, \mathrm{e}^{\mathrm{i}(\sigma_+-\sigma_j)} = 0. \tag{A 26d}$$

Solving (A 26*b*)–(A 26*d*) for the ratios α/Q, β/Q, h_+/Q, we have

$$\alpha/Q = -\frac{J_0(\epsilon_2) - \epsilon_2(\mathscr{H}_0/\mathscr{F})\{J_0(\epsilon_2) - \mathrm{i}J_1(\epsilon_2)\}}{\epsilon_1 \Delta}, \tag{A 27a}$$

$$\beta/Q = \frac{J_0(\epsilon_1) - \epsilon_1(\mathscr{H}_0/\mathscr{F})\{J_0(\epsilon_1) - \mathrm{i}J_1(\epsilon_1)\}}{\epsilon_2 \Delta}, \tag{A 27b}$$

$$h_+/Q = \frac{2}{\pi \Delta \mathscr{F}}[\epsilon_1 J_0(\epsilon_2)\{J_0(\epsilon_1) - \mathrm{i}J_1(\epsilon_1)\} - \epsilon_2 J_0(\epsilon_1)\{J_0(\epsilon_2) - \mathrm{i}J_1(\epsilon_2)\}], \tag{A 27c}$$

where Δ, $\mathscr{F}$, $\mathscr{H}_0$ are defined in equations (2.29)–(2.32).

The limit $\sigma_\pm \to \infty$

Consider the case $\sigma_\pm \to \infty$, ϵ_1, ϵ_2 finite, in which the displacement thickness waves have vanishingly small wavelengths. The asymptotic representations of the Hankel functions (Gradshteyn & Ryzhik 1980, p. 962) may be used to show that

$$G/\mathscr{F} \simeq O(1/\sigma_\pm), \quad \mathscr{H}_0/\mathscr{F} \simeq 2\mathrm{i}, \quad \mathscr{H}_1/\mathscr{F} \simeq 2. \tag{A 28}$$

Substituting in (2.28) we obtain

$$F(\epsilon) \simeq \frac{(\epsilon_2 - \epsilon_1)\{2\mathrm{i}(\epsilon_2 + \epsilon_1) - 1\}|J_0(\epsilon_1)|^2 + 2\{\epsilon_2^2 J_0(\epsilon_1) J_1(\epsilon_2) - \epsilon_1^2 J_0(\epsilon_2) J_1(\epsilon_1)\}}{\epsilon_1\epsilon_2[J_0(\epsilon_2) J_1(\epsilon_1) - J_0(\epsilon_1) J_1(\epsilon_2) + 2(\epsilon_2 - \epsilon_1)\{J_0(\epsilon_1) - \mathrm{i}J_1(\epsilon_1)\}\{J_0(\epsilon_2) - \mathrm{i}J_1(\epsilon_2)\}]}. \tag{A 29}$$

Taking $\nu = 0$ in this expression we recover equation (2.28) of I, which was derived in the absence of displacement thickness waves.

References

Betchov, R. & Criminale, W. O. 1967 *Stability of parallel flows*. New York: Academic Press.

Blake, W. K. 1970 *J. Fluid Mech.* **44**, 637–660.

Bull, M. K. 1967 *J. Fluid Mech.* **28**, 719–754.

Carrier, G. F., Krook, M. & Pearson, C. E. 1966 *Functions of a complex variable*. New York: McGraw-Hill.

Dowling, A. P., Ffowcs Williams, J. E. & Goldstein, M. E. 1978 *Phil. Trans. R. Soc. Lond.* A **288**, 321–349.

Ffowcs Williams, J. E. & Lovely, D. J. 1975 *J. Fluid Mech.* **71**, 689–700.

Gradshteyn, I. S. & Ryzhik, I. M. 1980 *Table of integrals, series and products* (corrected edn). New York: Academic Press.

Heller, H. H. & Bliss, D. B. 1975 *AIAA Pap.* 75–491.

Howe, M. S. 1980 *J. Fluid Mech.* **97**, 641–653.

Howe, M. S. 1981*a* *J. Fluid Mech.* **109**, 125–146 (Paper I.)

Howe, M. S. 1981*b* *Proc. R. Soc. Lond.* A **374**, 543–568.

Howe, M. S. 1981*c* *J. Sound Vib.* **75**, 239–250.

Howe, M. S. 1981*d* Bolt Beranek and Newman Tech. Memor AS16.

Laufer, J., Ffowcs Williams, J. E. & Childress, S. 1964 *AGARDOgraph* no. 90.

Liepmann, H. W. 1954 On the acoustic radiation from boundary layers and jets. Unpublished Rep., Guggenheim Aeronautics Laboratory, California Institute of Technology, Pasadena.

Michalke, A. 1965 *J. Fluid Mech.* **23**, 521–544.

Rockwell, D. & Naudascher, E. 1979 *A. Rev. Fluid Mech.* **11**, 67–94.

Ronneberger, D. 1972 *J. Sound Vib.* **24**, 133–150.

Ronneberger, D. 1980 *J. Sound Vib.* **71**, 565–581.

Tam, C. K. W. & Block, P. J. W. 1978 *J. Fluid Mech.* **89**, 373–399.

PHILOSOPHICAL TRANSACTIONS OF THE ROYAL SOCIETY A MATHEMATICAL, PHYSICAL & ENGINEERING SCIENCES